Geochimica et Cosmochimica Acta 364 (2024) 148–165

Contents lists available at ScienceDirect

Geochimica et Cosmochimica Acta

journal homepage: www.elsevier.com/locate/gca

Extremely deuterium depleted methane revealed in high-temperature volcanic gases

A. Ricci [a,*], J. Fiebig [b], F. Tassi [c,d], S. Hofmann [b], F. Capecchiacci [c,d,e], O. Vaselli [c,d]

[a] Istituto Nazionale di Geofisica e Vulcanologia, Sezione di Palermo, Via Ugo La Malfa, 153, 90146 Palermo, Italy
[b] Institute of Geosciences, Goethe University, Altenhöferallee 1, 60438 Frankfurt am Main, Germany
[c] Department of Earth Sciences, University of Florence, Via La Pira 4, 50121 Firenze, Italy
[d] CNR-IGG Institute of Geosciences and Earth Resources, Via La Pira 4, 50121 Firenze, Italy
[e] Istituto Nazionale di Geofisica e Vulcanologia, Sezione di Napoli, Osservatorio Vesuviano, Via Diocleziano, 328, 80124 Napoli, Italy

ARTICLE INFO

Associate editor: Shuhei Ono

Keywords:
Methane
Abiogenesis
Magmatic-hydrothermal fluids
Volcanic gases
Vulcano Island

ABSTRACT

Active volcanoes often discharge hot (T ≫ 100 °C) magmatic gases whose original composition has been modified through partial interaction with an externally fed hydrothermal system. The study of methane (CH_4) in these volcanic discharges may provide useful information on the interplay between deep magmatic gases and shallow circulation of hydrothermal fluids. However, the origin of CH_4 in high-temperature volcanic gases and the factors exerting control on its abundance and stable isotope composition are still largely unknown. Here, we present the abundances and stable isotopic composition of CH_4 in hot (99–387 °C) volcanic gases from the *La Fossa* volcanic crater of Vulcano Island (Southern Italy).

Our investigation revealed low (<1.5 μmol/mol) CH_4 concentrations and an extraordinarily large variability in CH_4 stable isotopic composition, with $\delta^{13}C$ and $\delta^{2}H$ values being positively correlated and varying from −35 to −9.2 ‰ and −670 to −102 ‰, respectively. Notably, CH_4 isotopes measured at Vulcano almost encompasses the global-scale variability observed in natural fluids, with $\delta^{2}H$ values ≤ −500 ‰ being the first ever reported in nature. Gases showing extremely negative $\delta^{13}C$-CH_4 and $\delta^{2}H$-CH_4 values systematically display higher CH_4 abundances.

We propose two possible scenarios in order to explain the observed huge variation in $\delta^{13}C$ and $\delta^{2}H$: (1) mixing of ^{13}C- and ^{2}H-depleted CH_4 with ^{13}C- and ^{2}H-enriched CH_4 of thermogenic origin formed under hydrothermal conditions; (2) post-genetic removal and isotopic alteration of ^{13}C- and ^{2}H-depleted CH_4 occurring during the ascent of volcanic gases. Comparing our dataset with available isotopic data from naturally occurring and artificially produced CH_4, a thermogenic origin for the isotopically light CH_4 seems unlikely. We postulate that the ^{13}C- and ^{2}H-depleted CH_4 may have formed via kinetically-controlled abiotic synthesis through CO (or CO_2) hydrogenation reactions in the hot ascending gas phase, possibly at temperatures intermediate between those typical of magmatic and hydrothermal conditions. Further investigations of methane in high-temperature volcanic gases are necessary to test this hypothesis.

1. Introduction

At active volcanoes, the interaction between magmatic gases (i.e., volatiles derived from degassing magma chambers) and an externally-fed hydrothermal phase occurring intermediate between the magma and the surface, play an important role in modulating the physical and chemical features of volcanic degassing at the surface. Fumarolic discharges whose original magmatic composition has been intensively modified through the interaction with a hydrothermal reservoir (i.e., so called hydrothermal gases) are characterized by the absence of acidic gas species, like SO_2, HCl and HF, due to extensive magmatic gas scrubbing (Symonds et al., 2001). Conversely, magmatic gases which only had limited interaction with a hydrothermal phase, in the following referred to as volcanic gases, still contain significant amounts of acid gases (e.g., SO_2). Methane is considered a key species to discriminate between hydrothermal gases, where it is usually present in relatively high concentrations (CO_2/CH_4 of $10–10^4$; Chiodini, 2009), and magmatic gases where thermodynamic calculations predict barely

* Corresponding author.
E-mail address: andrea.ricci@ingv.it (A. Ricci).

https://doi.org/10.1016/j.gca.2023.10.019
Received 17 May 2023; Accepted 12 October 2023
Available online 14 October 2023

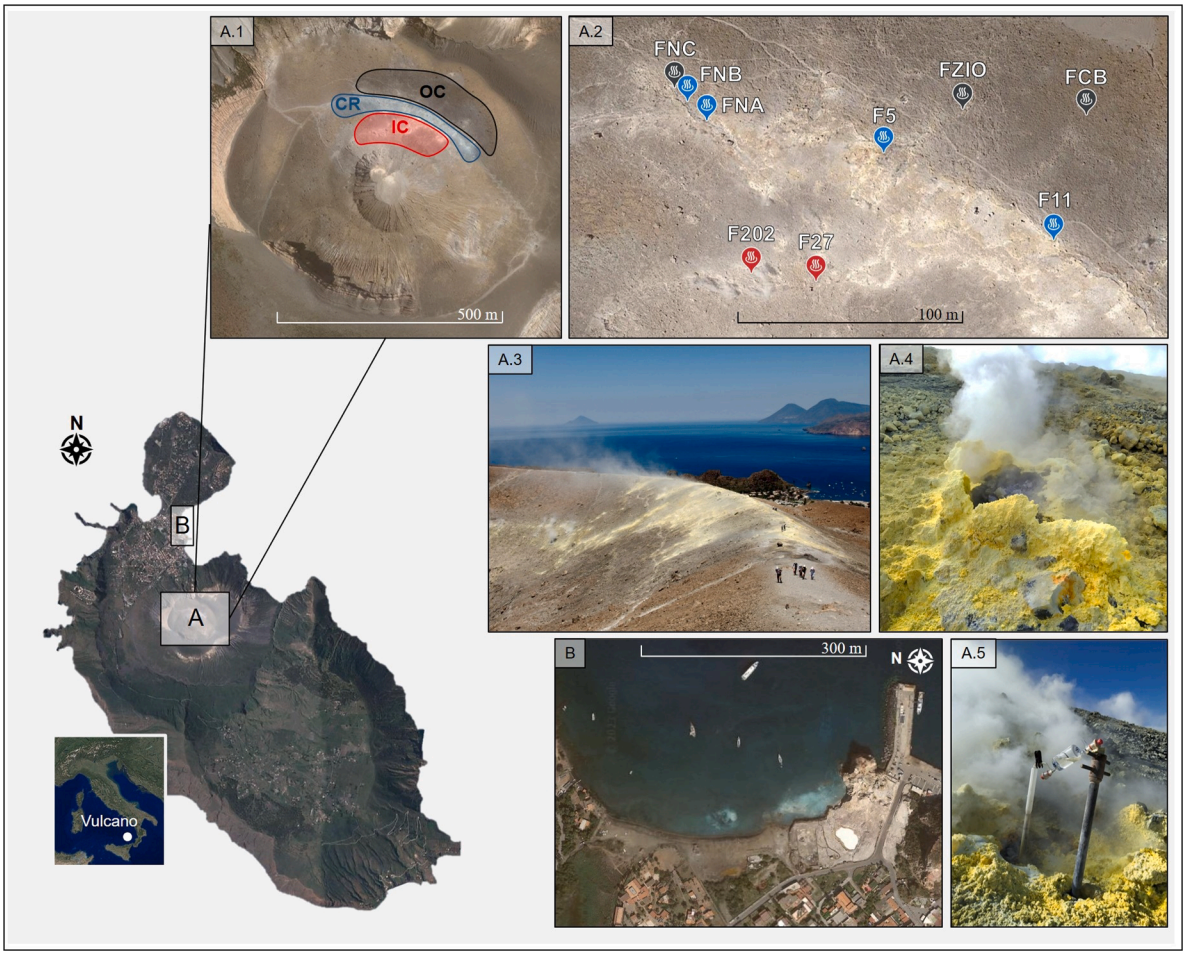

Fig. 1. Map of Vulcano Island showing the two main areas of degassing: *La Fossa* crater (A.1–A.5) and *Levante* beach (B). (A.1) Schematic division of the fumarolic field at the *La Fossa* crater into three main zones: IC = Inner Crater, CR = Crater Rim, and OC = Outer. (A.2) Locations of the sampled fumaroles with color-code as in panel (A.1). (A.3) Lateral view (from ESE to WNW) of the fumarolic field at the *La Fossa* crater; photo taken on June 2013. (A.4) Close-up photo of a high-temperature fumaroles located on the outer-crater area; photo taken on October 2022. (A.5) Photo of the sampling method (see Section 3.1. for further details). (B) Aerial view of the *Levante* beach area. The base maps used in the figure are from Google Earth.

detectable amounts ($CO_2/CH_4 = 10^6$–10^{12}; Chiodini, 2009). Volcanic gases typically contain low (≤1 μmol/mol), though detectable, amounts of CH_4 (Taran and Giggenbach, 2003). Consequently, the occurrence of CH_4 in volcanic gases has often been interpreted to record entrainment of fluids from the surrounding hydrothermal envelope into the central uprising flux of CH_4-poor magmatic gases (Taran and Giggenbach, 2003). Technical advances have recently made possible and feasible real-time continuous measurements of CH_4 abundance in volcanic gases using Multi-GAS systems equipped with a TDLS-based (Tunable Diode Laser Spectroscopy) CH_4 sensor (Salas-Navarro et al., 2022). However, the ability to grasp valuable information from such time series relies on accurate understanding of CH_4 formation mechanisms and conditions (i.e., abiotic synthesis vs. thermogenesis) and the effects of post-genetic processes (e.g., oxidative conversion; Taran and Giggenbach, 2003).

The stable isotopic composition of CH_4 represents an important tool for tracing the origin, secondary reactions, and transport of CH_4 in natural fluids (e.g., Etiope and Sherwood Lollar, 2013; Fiebig et al., 2019). Based on a global data set of carbon and hydrogen isotopes of CH_4 and C-isotopes on C_2–C_4 n-alkanes in emissions devoid of any acid magmatic components, the occurrence of CH_4 and light hydrocarbons in hydrothermal systems was predominantly ascribed to the thermal decomposition of organic matter under open-system conditions (Fiebig et al., 2019). However, Beaudry et al. (2021), by applying CH_4 clumped isotopologues and stable isotopes in hydrothermal fluids from Iceland and Nisyros Island (Greece), suggested that abiotic hydrocarbon formation via CO_2 reduction may be occurring at very high temperatures (>400 °C), for example at the magmatic-hydrothermal interface. At the venting surface, volcanic gases are commonly characterized by high temperatures, often exceeding 350 °C, and contain significant amounts of CO and H_2. These high temperatures and large availability of reactive surfaces (e.g., mineral and metal catalysts) could allow abiotic reactions to proceed by overcoming the high kinetic barriers of CO_2 hydrogenation (Giggenbach, 1997; Taran et al., 2007, 2010; McCollom et al., 2010, 2013, 2016).

Notwithstanding the relevant implications of deciphering the origin of CH_4, its extremely low concentrations in volcanic gases have impeded stable isotope analyses. As a result, to date, the stable isotope signature of CH_4 in volcanic gases is virtually unknown. A systematic review of available studies shows that carbon isotopic composition of CH_4 in such volcanic emissions has only been determined at five sites worldwide: White Island (New Zealand; Giggenbach, 1995), Mutnovsky volcano (Russia; Taran et al., 1992), Satsuma-Iwojima volcano (Japan; Sato et al., 1999, 2002), Guallatiri Volcano (Chile; Inostroza et al., 2020), and Damavand volcano (Iran; Zelenski et al., 2020). Similarly, the hydrogen isotopic composition of volcanic CH_4 is only reported from five locations: White Island (New Zealand; Giggenbach, 1995), Mounts Nasu, Mount Zaō, Mount Issaikyō, and Mount Kusatsu (Japan; Kiyosu, 1983). Interestingly, these studies show that carbon and hydrogen isotopic composition of volcanic CH_4 displays an extraordinarily large variability, with $\delta^{13}C$ and $\delta^{2}H$ ranging from −55.9 to −16.7 ‰ vs. V-PDB

and −487 to −99 ‰ vs. V-SMOW, respectively. Furthermore, the available datasets are extremely fragmentary and a robust set of observations from a single location is presently lacking. For example, combined $\delta^{13}C$ and $\delta^{2}H$ data of CH_4 has only been made available for one site (White Island). Therefore, it is still unknown which factors exert control on the observed isotopic variation.

Here, we present and discuss the abundances and isotopic compositions of CH_4 and co-discharged CO_2, C_2–C_3 hydrocarbons, H_2 and H_2O in hot (up to 400 °C) volcanic gases collected from the fumarolic field located in the northern sector of the *La Fossa* volcanic crater (Vulcano Island, Aeolian Archipelago, Southern Italy; Fig. 1). Vulcano, one of the most studied active volcanoes worldwide (Inguaggiato et al., 2018), is characterized by an intense fumarolic activity sourced by a magmatic-hydrothermal fluid mixture (Chiodini et al., 1993; Taran, 2011; Paonita et al., 2013). Its high-temperature discharged vapors contain low concentrations of CH_4 and higher hydrocarbons (e.g., Capasso et al., 1997; Giggenbach et al, 2001; Tassi et al., 2012; Paonita et al., 2013; Schwandner et al., 2013), and high-temperature vents are easily accessible. This makes Vulcano Island an ideal site for studying the C—H isotope systematics and the origin of CH_4 in volcanic gases and identifying the factors controlling its abundance and stable isotopic composition.

2. The magmatic-hydrothermal system of the *La Fossa* crater at Vulcano Island (Southern Italy)

Vulcano Island is the southernmost island of the Aeolian Archipelago in the Tyrrhenian Sea (Fig. 1). The Aeolian islands are the exposed summits of volcanic edifices which, together with the surrounding seamounts, constitute a volcanic arc related to the subduction of the Ionian slab underneath the Calabro-Peloritani terrain (e.g., Zanon et al., 2003). The current geomorphology of Vulcano Island was interpreted as the result of eruptive periods of at least three volcanic complexes separated by volcano-tectonic events and major quiescence stages (De Astis et al., 1997; Nicotra et al., 2018). The present fumarolic discharges mostly occur at the top of the main volcanic cone in a 0.045 km^2 wide area (Aiuppa et al., 2005) located in the northern sector of the so-called *La Fossa* crater (Casalbore et al., 2019) where high temperature vents (up to 400 °C) discharge volcanic gases rich in CO_2 and acidic species (SO_2, H_2S, HCl and HF). After the last 1888–1890 eruptive phase, the *La Fossa* crater experienced numerous episodes of volcanic unrest (Selva et al., 2020), the most recent of which started in summer 2021 and is still ongoing (Federico et al., 2023). Such events were characterized by rising vent temperatures (Sicardi, 1941; Cannata et al., 2012; Harris et al., 2012; Diliberto, 2017) and volatile fluxes (Italiano et al., 1998, Granieri et al., 2006), expansion of the fumarolic field, strong and relatively quick changes in the chemical and isotopic composition of the discharged fluids (Chiodini et al., 1996; Capasso et al., 1997; Paonita et al., 2013; Aiuppa et al., 2022) and changes in the diffuse soil CO_2 flux and geochemistry of thermal aquifers in the areas surrounding the volcanic cone (Capasso et al., 1999, 2001, 2014; Diliberto et al., 2021; Di Martino et al., 2022; Inguaggiato et al., 2022). Despite the geochemical and geophysical signals of renewed activity recorded during these unrest periods, none of the volcanic crises culminated with paroxysmal events.

During the last four decades, Vulcano Island has been subject of several investigations focused on elaborating a reliable geochemical model of the fumarolic system, a crucial factor in correctly interpreting geochemical signals as eruption precursors (e.g., Chiodini et al., 1995; Leeman et al., 2005; Paonita et al., 2013). Among the different models proposed (Martini and Tonani, 1970; Martini et al., 1980; Carapezza et al., 1981; Cioni and D'Amore, 1984; Nuccio et al., 1999), there is a general consensus in considering the composition of the crater fumaroles as the result of a mixing between magmatic gases and hydrothermal fluids. The inferred magmatic component is characterized by high CO_2, N_2 and He contents (up to around 30 mol%, 1400–3000 μmol/mol and 3 μmol/mol, respectively), low H_2O concentrations (≤70 mol%),

Table 1
Name, location, sampling temperatures and gas chemistry of the investigated fumaroles from the *La Fossa* crater (Vulcano Island, Southern Italy). The chemical composition is reported in μmol/mol; na: not available. IC = inner crater ([a]); CR = crater rim ([b]); OC = outer crater ([c]).

Fumarole name	Fumarole location	Latitude °N	Longitude °E	Sampling Date mm-yyyy	$T^{samp.}$ °C	Sample ID	H_2O	CO_2	SO_2	H_2S	S^{tot}	HCl	HF	H_2	O_2	N_2	Ar	He	CO	CH_4
F202	IC[a]	38.405526	14.961665	05-2017	202	F202a	892,000	96,238	6048	3024	9072	313	5.0	93	0.10	2268	0.80	0.17	9.50	0.39
F202	IC	38.405526	14.961665	07-2017	na	F202b	na	na	na	na	na	na	na	na	na	na	na	na	na	na
F27	IC	38.405493	14.962009	05-2015	222	F27a	869,000	119,587	4323	3406	7729	421	3.4	111	0.88	3144	1.70	0.41	1.83	0.28
F27	IC	38.405493	14.962009	05-2017	199	F27b	883,000	98,514	7956	5967	13,923	363	8.0	90	0.14	4212	1.06	0.26	9.01	0.18
FNA	CR[b]	38.406157	14.961490	05-2015	387	FNAa	890,000	98,470	5362	4158	9520	131	1.9	121	0.42	1751	2.75	0.28	1.04	0.17
FNA	CR	38.406157	14.961490	06-2016	na	FNAb	864,000	119,730	7888	5576	13,464	286	11.6	56	0.10	2448	1.18	0.46	2.99	0.15
FNA	CR	38.406157	14.961490	05-2017	340	FNAc	879,000	109,154	5324	3993	9317	266	4.4	70	0.13	2178	0.93	0.25	8.59	0.25
FNA	CR	38.406157	14.961490	11-2021	342	FNAd	837,000	154,000	5700	1310	7010	1130	75.0	36	0.34	489	0.81	1.50	0.35	0.11
FNB	CR	38.406234	14.961391	05-2017	325	FNB	905,000	85,591	4845	2470	7315	238	4.0	39	0.08	1805	0.58	0.28	7.13	0.31
FNC	OC[c]	38.406289	14.961318	10-2016	220	FNC	875,000	115,687	3250	3125	6375	163	1.9	14	0.30	2750	0.98	0.33	7.63	0.26
F5	CR	38.406031	14.962387	10-2016	362	F5a	892,000	95,779	6048	3348	9396	302	3.9	28	0.62	2484	1.00	0.48	3.67	0.59
F5	CR	38.406031	14.962387	05-2017	351	F5b	875,000	115,333	4500	2750	7250	363	6.4	36	0.16	2000	0.86	0.19	9.75	0.61
F11	CR	38.405692	14.963233	06-2016	na	F11a	893,000	88,385	10,448	6292	16,740	309	3.7	61	0.10	1498	1.06	0.88	1.42	0.08
F11	CR	38.405692	14.963233	05-2017	299	F11b	888,000	98,388	6832	3808	10,640	403	9.7	86	0.12	2464	0.96	0.15	7.73	0.15
FCB	OC	38.406182	14.963430	11-2021	270	FCB	855,000	136,000	5400	1500	6900	1430	85.0	18	8.60	923	1.90	1.10	0.16	0.31
FZIO	OC	38.406204	14.962784	06-2016	99	FZIOa	909,000	85,764	1183	1183	2366	171	2.1	56	0.10	2639	0.71	0.26	1.00	0.15
FZIO	OC	38.406204	14.962784	10-2016	99	FZIOb	912,000	83,085	968	1056	2024	136	1.9	18	0.36	2728	0.57	0.16	4.84	0.07
FZIO	OC	38.406204	14.962784	05-2017	99	FZIOc	905,000	90,047	1520	1045	2565	171	2.0	23	0.18	2185	0.84	0.26	5.51	0.08

Table 2
Hydrocarbon concentration ratios of volcanic gases collected at the *La Fossa* crater (Vulcano Island, Southern Italy) between 2015 and 2021. The sum of alkanes and alkenes having the same carbon number is expressed as C_2^{tot} ($C_2H_6 + C_2H_4$) and C_3^{tot} ($C_3H_8 + C_3H_6$).

Fumarole name	Sampling Date mm-yyyy	Sample ID	CH_4/C_2H_6	C_2H_6/C_3H_8	C_2H_4/C_2H_6	C_3H_6/C_3H_8	$CH_4/(C_2H_6 + C_2H_4)$	$CH_4/(C_2^{tot} + C_3^{tot})$
F202	05-2017	F202a	346		0.7		203	
F202	07-2017	F202b	185	1.1	4.4	8.3	34	13
F27	05-2015	F27a	239	12.6	0.2	2.0	198	165
F27	05-2017	F27b						
FNA	05-2015	FNAa	484		1.1		231	
FNA	06-2016	FNAb	133		2.5		38	
FNA	05-2017	FNAc	171					
FNA	11-2021	FNAd	150	1.9	0.5	1.0	100	59
FNB	05-2017	FNB						
FNC	10-2016	FNC	129		8.8		13	
F5	10-2016	F5a	591		1.7		220	
F5	05-2017	F5b	30		0.8		17	
F11	06-2016	F11a	99		4.6		18	
F11	05-2017	F11b						
FCB	11-2021	FCB	822		1.2		381	
FZIO	06-2016	FZIOa	83		1.7		31	
FZIO	10-2016	FZIOb	95		2.2		30	
FZIO	05-2017	FZIOc	91		1.1		43	

Table 3
Stable isotopic composition of volcanic gases collected at the *La Fossa* crater (Vulcano Island, Southern Italy) between 2015 and 2021. Isotopic compositions of H and C are reported in delta notation (‰) relative to V-SMOW and V-PDB, respectively. The isotopic composition of the total C_2 and C_3 fraction (C_2^{tot}, C_3^{tot}) is calculated according to mass conservation equation: $\delta^{13}C\text{-}C_ntot = \delta^{13}C\text{-}C_nH_{2n+2} \times (x) + \delta^{13}C\text{-}C_nH_{2n} \times (1\text{-}x)$, where x is the mole fraction of C_nH_{2n+2}. The difference between the carbon isotopic composition of two gas species is reported as $\Delta^{13}C$. When the carbon isotopic composition of CO_2 is not available, the average $\delta^{13}C$ value is used to calculate the $\Delta^{13}C$ value.

Fumarole name	Sampling Date mm-yyyy	Sample ID	δ^2H (‰ vs. V-SMOW)			$\delta^{13}C$ (‰ vs. V-PDB)								$\Delta^{13}C$ (‰ vs. V-PDB)	
			H_2O	H_2	CH_4	CO_2	CH_4	C_2H_6	C_3H_8	C_2H_4	C_3H_6	C_2^{tot}	C_3^{tot}	CO_2–CH_4	CH_4–C_2^{tot}
F202	05-2017	F202a	8	−627	−646	−0.5	−27.2	−28.3						26.7	
F202	07-2017	F202b					−20.8	−20.5	−21.9	−25.8	−16.3	−24.8	−16.9	20.1	4.0
F27	05-2015	F27a					−27.7	−28.5	−31.1	−31.4	−31.7	−29.0	−31.5	27.0	1.3
F27	05-2017	F27b	1		−116	−0.5	−9.4							8.9	
FNA	05-2015	FNAa				−0.9	−28	−27.4		−28.6		−28.0		27.1	0.03
FNA	06-2016	FNAb			−394	−0.8	−19.6	−20.8		−26.1		−24.6		18.8	5.0
FNA	05-2017	FNAc	4	−299	−586	−0.4	−26.1	−21.1						25.7	
FNA	11-2021	FNAd			−102	0.2	−9.2	−14.5						9.4	
FNB	05-2017	FNB	12	−592	−257	−0.3	−21.7							21.4	
FNC	10-2016	FNC	1	−553	−214	−0.8	−11.5	−13.6		−24.4		−23.3		10.7	11.8
F5	10-2016	F5a	−1	−525	−657	−1.1	−29	−27.3		−26.7		−26.9		27.9	−2.1
F5	05-2017	F5b	6	−347	−157	−0.7	−29.7	−26.6						29.0	
F11	06-2016	F11a			−143	−1.1	−11.2	−13		−16.6		−16.0		10.1	4.8
F11	05-2017	F11b	2	−638		−0.9	−23.2							22.3	
FCB	11-2021	FCB			−670		−35	−28.6						34.3	
FZIO	06-2016	FZIOa				−1.2	−23.6	−22.5		−26		−24.7		22.4	1.1
FZIO	10-2016	FZIOb	−27		−147	−1.1	−12.9	−15.1		−24.2		−21.4		11.8	8.5
FZIO	05-2017	FZIOc	−38		−185	−0.9	−21.4							20.5	

Table 4
Hydrocarbon concentration ratios and stable isotope composition of methane and ethane of gases collected from fumarole F5b (i.e., fumarole F5 sampled on May 2017) with or without using the titanium tube.

Fumarole F5b			
Measured parameters	Sampled with titanium tube	Sampled without titanium tube	Average values
CH_4/C_2H_6	31.7	28.9	30.3
C_2H_4/C_2H_6	0.75	0.89	0.82
$CH_4/(C_2H_6 + C_2H_4)$	18.1	15.3	16.7
$\delta^2H\text{-}CH_4$ (‰ vs. V-SMOW)	−163	−152	−157
$\delta^{13}C\text{-}CH_4$ (‰ vs. V-PDB)	−29.2	−30.2	−29.7
$\delta^{13}C\text{-}C_2H_6$ (‰ vs. V-PDB)	−25.3	−27.8	−26.6

and $\delta^2H\text{-}H_2O$ of around −15 ‰ vs. V-SMOW, resembling the chemical and isotopic features of a typical subduction-related andesitic water (Giggenbach, 1992). Several authors (e.g., Tedesco and Scarsi, 1999; Taran, 2011; Paonita et al., 2002, 2013) showed that the CO_2-rich end-member also has high $^3He/^4He$ ratios (R/R_a up to 6.0), $\delta^{13}C\text{-}CO_2$ of 0 ± 0.5 ‰, and low $^{40}Ar/^{36}Ar$ values (≈300–400), which are similar to those measured in fluid inclusions hosted in olivine and clinopyroxene from the recently erupted volcanic rocks (Magro and Pennisi, 1991; Mandarano et al., 2016). The hydrothermal component is instead characterized by higher H_2O (≈95 mol%), lower CO_2 (≈3–5 mol%), $\delta^2H\text{-}H_2O$ of around 0 ± 10 ‰, lower $\delta^{13}C\text{-}CO_2$ (−3 ‰), significantly lower amounts of N_2 and He (around 200 and 0.1 μmol/mol, respectively), high N_2/Ar values (≈1000), and an excess of radiogenic isotopes (^4He, ^{40}Ar, ^{21}Ne and ^{22}Ne), suggesting a marked crustal signature (Chiodini et al., 1995; Tedesco and Scarsi 1999; Paonita et al., 2002, 2013; Taran, 2011). Based on the isotopic composition of fumarolic condensates, a marine origin of the water sourcing the hydrothermal system has been inferred by several authors (e.g., Chiodini et al., 2000; Paonita et al.

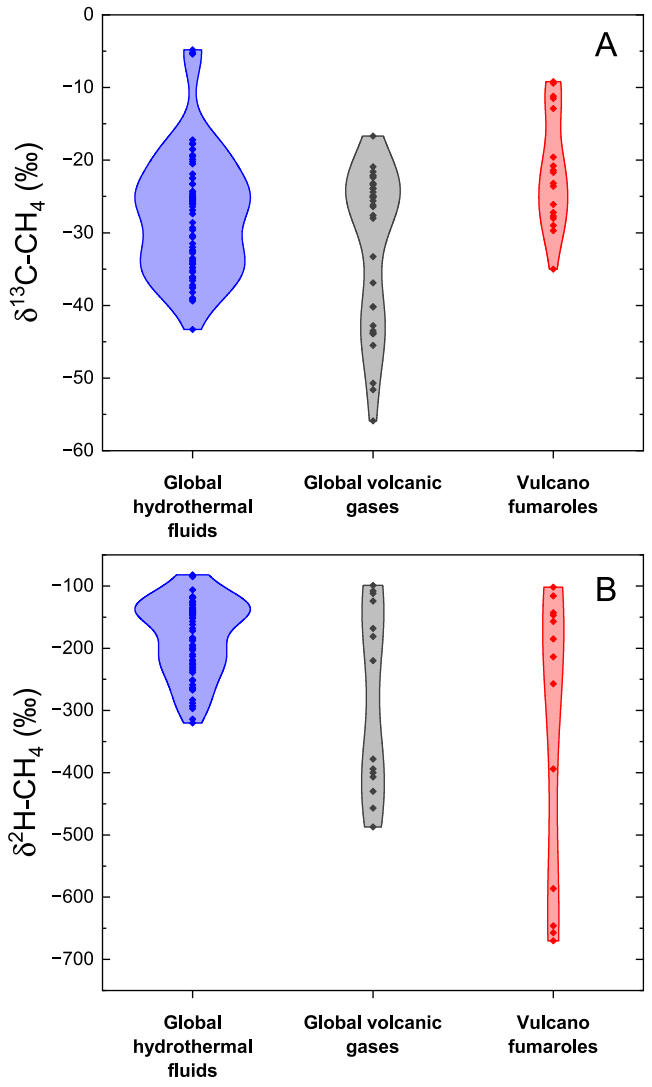

Fig. 2. Violin plots showing the carbon (A) and hydrogen (B) isotopic composition of CH_4 in hydrothermal fluids (Fiebig et al., 2019); global volcanic gases (Table S2) and fumarolic gases discharged at the La Fossa crater of Vulcano Island (Table 3). Shaded regions behind data points delineate sample frequency and are generated using the Kernel smoothing approach. Measured isotopic values are reported as solid diamonds. The isotopic compositions are reported in delta notation (‰) relative to V-PDB and V-SMOW for carbon and hydrogen, respectively.

2002; Leeman et al., 2005). Along with the magmatic and hydrothermal components, minor contributions from meteoric water have been hypothesized to occasionally contaminate the fumarolic gases (Chiodini et al., 1995; Capasso et al., 1997; Tedesco and Scarsi, 1999; Paonita et al., 2002; Taran, 2011).

3. Materials and methods

3.1. Gas sampling

Gas samples from 9 fumaroles (Fig. 1) were collected in May 2015, June 2016, October 2016, May 2017 and November 2021. During this time span, six fumaroles were sampled multiple (2–4) times. The sampled fumaroles are located along the fractures that extend outwards from the rim (FNC, FCB and FZIO), on the rim itself (FNA, FNB, F5 and F11) and in the inner part of the rim (F27 and F202) of the *La Fossa* crater. Venting temperatures were highest for those on the rim (from 299 to 387 °C), medium for the ones at the inner part of the crater (199–222 °C) and highly variable for outer-rim fumaroles (99–270 °C). Sampling of volcanic gases was performed following the protocols described in Vaselli et al. (2006). At fumarolic vents, pre-evacuated 60 mL glass flasks, equipped with a Teflon stopcock and filled with 20 mL of 4 N NaOH and 0.15 M $Cd(OH)_2$ solution (Montegrossi et al., 2001) were used in line with a titanium tube and double-wall glass Dewar tubes to sample gases for determination of bulk gas composition. In order to evaluate the potential late generation of CH_4 through the interaction of fumarolic gases with the titanium tube at the metal-gas interface, an additional gas sample has been collected at fumarole F5 in May 2017 by directly inserting the glass line into the ground. During sampling, water vapor and acidic gas species (CO_2, SO_2, HCl and HF) dissolved in the soda solution, whereas H_2S precipitated as insoluble CdS. Low-solubility gas compounds, such as N_2, O_2, CO, H_2, He, Ar, CH_4 and light hydrocarbons, were concentrated in the sampling flask headspace. Steam condensates (for the analysis of the $^2H/^1H$ ratio of H_2O) and dry gases (for the analysis of $^{13}C/^{12}C$ ratio of CO_2 and $^2H/^1H$ ratio of H_2) were sampled using a water-cooled condenser connected to the sampling line adopted for the soda flasks. At each sampling site, an additional gas sample was collected in 100–250 mL glass flasks filled with 30–80 mL of 4 N NaOH solution for the analysis of $^{13}C/^{12}C$ ratios of CH_4 and C_{2+} hydrocarbons and $^2H/^1H$ ratio of CH_4 and the determination of relative abundances of C_1–C_3 hydrocarbons.

3.2. Chemical and isotopic analyses

The concentration of CH_4 and inorganic gas species (H_2O, CO_2, SO_2, H_2S, HCl, HF, N_2, Ar, O_2, He, CO) was determined by ion chromatography (IC) and gas chromatography (GC) at the Department of Earth Sciences at the University of Florence (Italy). The inorganic compounds stored in the sampling flask head-space were analyzed by a Shimadzu 15A gas-chromatograph equipped with a thermal conductivity detector (TCD), using a 10 m long stainless-steel packed molecular sieve column and helium or argon (the latter being used for He analysis) as carrier gases. Argon and O_2 were analyzed using a Thermo Focus gas chromatograph Equipped with a 30 m long capillary molecular sieve column and a TCD (Vaselli et al., 2006). The caustic solution was separated from solid CdS by centrifugation, oxidized with H_2O_2, and used for the analysis of: 1) CO_2 as CO_3^{2-} by automatic titration with 0.5 M HCl (Metrohm 794 Basic Titrino), and 2) HF, HCl and SO_2 as F^-, Cl^- and SO_4^{2-} by IC (Metrohm 761 Compact IC), respectively. Solid CdS was then dissolved with H_2O_2 to analyse H_2S as SO_4^{2-} by IC (Montegrossi et al., 2001). The analytical errors for GC and IC analyses were better than 5 %.

The stable isotopic composition of CH_4, light hydrocarbons, CO_2, H_2 and water was analyzed in the Stable Isotope Laboratory at Goethe University Frankfurt (Germany). The carbon isotopic composition of CO_2 was analyzed using a Flash-EA 1112 (Thermo) interfaced with a MAT 253 isotope ratio mass spectrometer according to the protocol provided in Fiebig et al. (2004, 2007). Reproducibility was better than ±0.2 ‰. Carbon isotope analysis of CH_4 and light hydrocarbons were performed using analytical setups and protocols described by Fiebig et al. (2015, 2019). Gas samples were injected into to a GC-C-II (Thermo), equipped with GC column GS CarbonPlot (Agilent), which was connected to the continuous flow inlet system of a Thermo Scientific MAT 253 ‘gas source’ mass spectrometer. In order to generate mass spectrometric signals for accurate and precise carbon isotope analysis, all gas samples encompassed a preconcentration line equipped with two cryofocus units, packed with Porapack Q (50–80 mesh), before being injected into the GC column. External precision was ±0.5 ‰. Concentrations of C_2-C_3 hydrocarbons relative to methane were determined from the peak areas of mass spectrometric chromatograms, comparing ratios of peak areas of samples with those of a standard with known absolute concentrations of C_1–C_4 hydrocarbons. Analytical precision for hydrocarbon concentration ratios was ≤±10 %. The hydrogen isotope analysis of CH_4 was carried out using analytical setups described in Fiebig et al. (2019). Methane was first preconcentrated using the setup

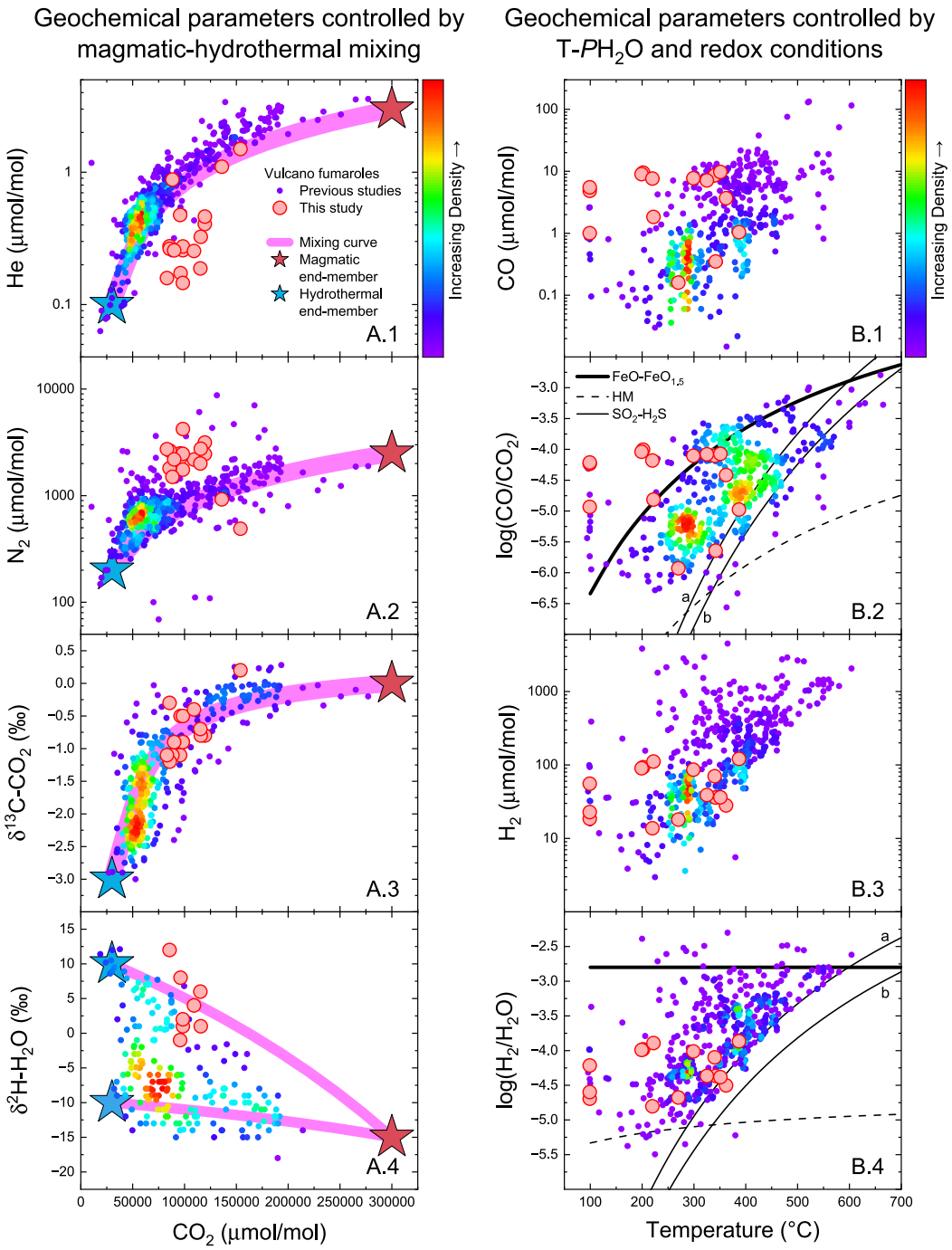

Fig. 3. Biplots of CO_2 versus He (A.1), N_2 (A.2), $\delta^{13}C$-CO_2 (A.3) and δ^2H-H_2O (A.4), and outlet temperatures versus CO (B.1), log(CO/CO_2) (B.2), H_2 (B.3) and log (H_2/H_2O) (B.4) for volcanic gases discharged by the crater fumaroles of Vulcano Island. Data are from previous studies (Table S1) and this work (Tables 1 and 3). Biplots in the left column (A) show the geochemical parameters that are interpreted (e.g., Chiodini et al., 1995, Taran, 2011, Paonita et al., 2013) to be controlled by a mixing process (light-purple curves) between magmatic volatiles (red star) rich in CO_2 and CO_2-poor hydrothermal fluids (sky-blue star). Based on previous studies (e.g., Taran, 2011; Paonita et al., 2013), values of CO_2 (µmol/mol), He (µmol/mol), N_2 (µmol/mol), $\delta^{13}C$-CO_2 (‰ vs. V-PDB) and δ^2H-H_2O (‰ vs. V-SMOW) are assumed to be 300000, 3, 2500, +0 and –15, and 30000, 0.1, 200, –3 and –10 to +10 for the magmatic and hydrothermal end-member, respectively. On the contrary, in the right column (B) geochemical parameters considered to be controlled by temperature, pressure (PH_2O) and redox conditions (e.g., Chiodini et al., 1993, 1995) are shown. Theoretical curves of equilibrium values of log(CO/CO_2) and log(H_2/H_2O) in function of temperature at different redox conditions (i.e., FeO-$FeO_{1.5}$, Hematite-Magnetite and SO_2-H_2S) are reported for comparison. The relevant functions of the applied redox buffers are from and Capaccioni et al. (2004). The theoretical curves of SO_2-H_2S gas buffer are computed for PH_2O of 1 bar and SO_2/H_2S ratio of 0.5 (a) and 15 (b). Our data well compare with previous measurements. The only notable exception is helium which, in most of the samples, shows lower concentrations than those commonly found when CO_2 contents are around 100000 µmol/mol. This might be caused by time-dependent loss of helium via diffusion through the glass walls of the sample storage flasks having occurred before the gas chromatographic analysis. Our gas samples were not meant for volcanic surveillance purposes and, therefore, there was no need to minimize the sampling-measurement time interval. Data from previous studies are shown with symbols having colors assigned based on the density of data points in the scatter plots. The color-scale is shown as colored vertical columns. This setting helps visualizing where the most frequent measured compositions are.

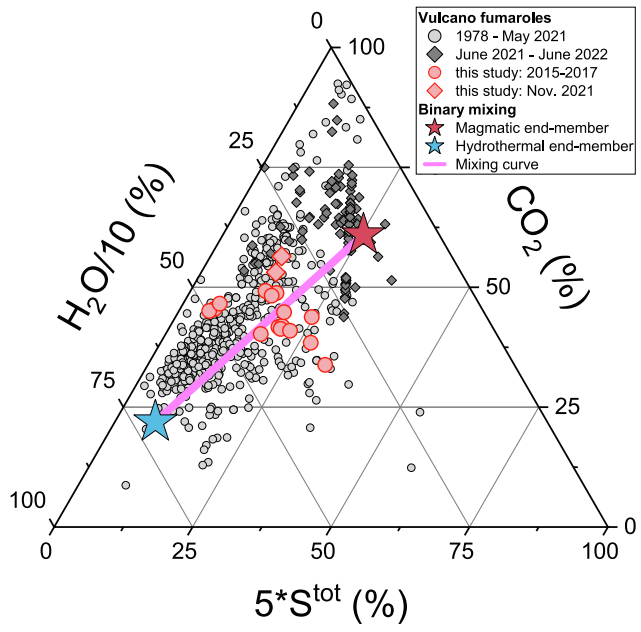

Fig. 4. CO_2-H_2O-S^{tot} (where $S^{tot} = SO_2 + H_2S$) ternary scatter plot showing the gas composition of volcanic gases discharged at the La Fossa crater of Vulcano Island during the last episode of unrest (data from June 2021 until June 2022; circles) and in the previous decades (data from 1978 to May 2021; diamonds). Data from previous studies are from both Multi-GAS measurements and direct sampling of fumaroles (Table S1). Our data well compare with previous measurements and also show an increase in CO_2 and, to a lesser extent, S^{tot} contents during the last episode of unrest as reported by other studies (Aiuppa et al., 2022, Federico et al. 2023). The compositional trend is commonly interpreted as the result of a mixing process (light-purple curve) between a H_2O-rich hydrothermal component (sky-blue star) and magmatic volatiles higher in CO_2 and S^{tot} (red star). Total sulfur (S^{tot}), CO_2 and H_2O concentrations (in mol%) of 2.5, 30 and 67.5 and 0.2, 3 and 96.8 have been used for the magmatic and hydrothermal end-member, respectively. There is no consensus in the literature on the actual composition of the two end-members, hence, different sets of values can also be used (e.g., magmatic gases with slightly higher total sulfur contents). However, this is expected to cause only minor changes.

outlined above for the carbon isotope analysis, separated from H_2, N_2 and CO by cooling the GC column down to −30 °C and keeping it isothermal during measurements and finally introduced into a MAT 253 gas source mass spectrometer (Thermo Finnigan) using He as carrier gas. External precision for δ^2H-CH_4 analysis was ≤±5 ‰. Determination of $^2H/^1H$ ratio in H_2 was performed following the analytical protocols outlined by Ricci et al. (2022). A variable amount of dry gas sample was expanded into a sample loop having a fixed volume (100 µl) through a pre-evacuated injection line. The sample was then transferred towards the GC column (Molecular sieve 5A) by means of an He carrier gas flow. H_2 was separated from the other gas compounds by holding the column at −50 °C. The hydrogen isotope ratios were then determined from the 3/2 intensity ratios (HD/H_2) of sample H_2 compared to that of a reference gas with known isotopic composition, calibrated against the primary reference standard V-SMOW. In order to be able to correct for scale contraction, different H_2-standards with known isotopic composition were analyzed along with the samples [+133.7 ‰ (OzTech), −366 ‰ (OzTech) and −710 ‰, all vs. V-SMOW]. A further correction was applied to the hydrogen stable isotope analysis to remove the mass 3 contribution from H_3^+-ion produced in the source (Sessions et al., 2001). Internal reproducibility was better than ±5 ‰ (1σ). The analysis of the hydrogen isotopic composition of water was performed on a TC-EA (Thermo Finnigan) coupled with a MAT 253 stable isotope ratio mass spectrometer. The external precision was better than ±3 ‰ (1σ). The measured stable isotopic compositions are reported in delta notation (‰) relative to V-PDB and V-SMOW for carbon and hydrogen, respectively.

4. Results

4.1. Chemical gas composition

Geographical coordinates, sampling date, outlet temperatures, bulk chemical composition and hydrocarbon concentration ratios of collected volcanic gases from Vulcano are reported in Tables 1 and 2.

The principal constituent of fumarolic gases is H_2O (>837000 µmol/mol) followed by CO_2 (83085–154000 µmol/mol). Contents of acidic gases, namely SO_2, H_2S, HCl and HF, are up to 10448 µmol/mol, 6292 µmol/mol, 1430 µmol/mol and 85 µmol/mol, respectively. N_2 and H_2 contents range from 489 to 4212 µmol/mol and from 14 to 124 µmol/mol, respectively. Ar, O_2, He, and CO vary between 0.57 and 2.75 µmol/mol, 0.08 and 8.6 µmol/mol, 0.15 and 1.5 µmol/mol, and 0.16 and 9.75 µmol/mol, respectively. Methane contents are relatively low and range from 0.07 to 0.61 µmol/mol. Based on the hydrocarbon concentration ratios, contents of ethane (C_2H_6) and ethene (C_2H_4) were determined for 14 and 13 samples, respectively and are found to vary between 0.3 and 20.4 nmol/mol, and 0.2 and 17.9 nmol/mol, respectively. Concentrations of propane (C_3H_8) and propene (C_3H_6) range from 0.1 to 0.4 nmol/mol and from 0.2 to 0.4 nmol/mol, respectively.

4.2. Carbon isotopic composition of CO_2, CH_4 and C_2–C_3 hydrocarbons

Carbon isotopic composition of C-bearing gas compounds in volcanic gases discharged at Vulcano are listed in Tables 3 and 4. δ^{13}C-CO_2 extends from −1.2 to +0.2 ‰, in good agreement with the isotopic range (−3 to +0.5 ‰) reported by Paonita et al. (2013) for the 1988–2009 period. Carbon isotopic composition of CH_4 displays a large variation, with δ^{13}C-CH_4 values varying from −35 to −9.2 ‰. It is worth noting that the carbon isotopic composition of CH_4 for a given vent location is not constant over time. For example, at F27 and FNA vents large isotopic variations of up to around 18 ‰ are observed over a 2- and 4-year period, respectively. Furthermore, the extraordinary wide range of δ^{13}C-CH_4 values reported for the Vulcano gases cover around 70 % of the current global variability observed in terrestrial hydrothermal fluids (Fiebig et al., 2019; Fig. 2A). Light hydrocarbons also show a highly variable carbon isotopic composition. The δ^{13}C values of C_2H_6, C_3H_8, C_2H_4 and C_3H_6 vary between −28.6 and −13 ‰, −31.1 and −21.9 ‰, −31.4 to −16.6 ‰, and −31.7 and −16.3 ‰, respectively.

4.3. Hydrogen isotopic composition of H_2O, H_2 and CH_4

Hydrogen isotopic composition of H_2O (water vapor), H_2 and CH_4 in Vulcano gases are reported in Tables 3 and 4. δ^2H-H_2O of most condensates of Vulcano crater ranges from −1 to +12 ‰ vs. V-SMOW, i.e., within the range (−20 to +15 ‰) already observed at Vulcano in previous studies (e.g., Paonita et al., 2013). Fumarole FZIO exhibits significantly more negative δ^2H-H_2O values (−32.5 ± 5.5 ‰ vs. V-SMOW), possibly indicating steam condensation or shallow meteoric water addition, as also suggested by its lower venting temperatures (99 °C) and more peripheral position compared to the other crater fumaroles (Fig. 1). δ^2H-H_2 and δ^2H-CH_4 vary considerably from −638 to −299 ‰ vs. V-SMOW, and −670 to −102 ‰ vs. V-SMOW, respectively (Table 3). Notably, the range of δ^2H-CH_4 measured at Vulcano encompasses the global-scale variability observed in nature (Milkov and Etiope, 2018), with δ^2H values ≤ −500 ‰ being, to the best of our knowledge, the lowest isotopic values ever reported (Fig. 2B).

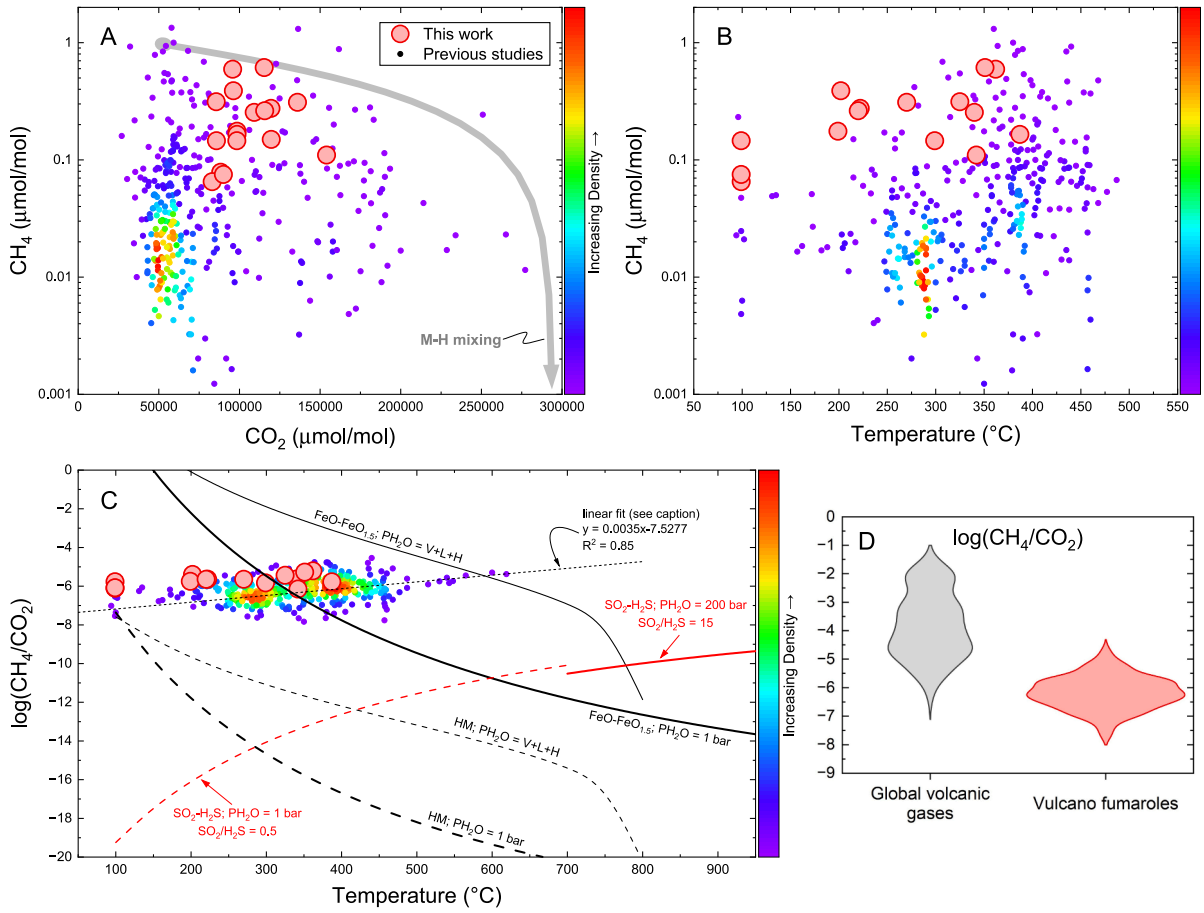

Fig. 5. Evaluation of factors controlling CH_4 abundances in the volcanic gases discharged from the Vulcano crater fumaroles. Data are from this study (red-edged circles, Table 1) and previous measurements reported elsewhere (Table S1). The latter dataset is reported as colored circles, with colors assigned based on the density of data points in the scatter plots (color-scale as vertical columns). (A) Biplot of CO_2 (µmol/mol) versus CH_4 (µmol/mol). Mixing between CH_4-bearing (1 µmol/mol) and CO_2-poor (50000 µmol/mol) hydrothermal fluids and CH_4-devoid and CO_2-rich (300000 µmol/mol) magmatic gases is shown as a solid gray arrow (M-H mixing). (B) Biplot of outlet gas temperatures versus CH_4 concentrations. A weak direct correlation can be seen. (C) Biplot of outlet gas temperatures versus measured $\log(CH_4/CO_2)$ ratios. Two clusters of data are identified with central T-log coordinates of 283 °C and –6.61, and 390 °C and –6.03, respectively. The best linear fit (short-dashed black line) is computed considering the central points of the two above-mentioned clusters and the T-log values of the data having temperatures ≥500 °C. Theoretical equilibrium curves computed for different T-PH_2O-fO_2 conditions are shown for comparison. Solid and dashed red curves describe temperatures, pressures and redox conditions prevailing in the deep magmatic gases and close to the surface at vents, respectively. Solid and dashed black curves depict the variation of $\log(CH_4/CO_2)$ equilibrium values with temperature, calculated for redox conditions governed by rock buffers (FeO-$FeO_{1.5}$ and Hematite-Magnetite) and at water pressure (PH_2O) of 1 bar or fixed by the vapor–liquid-halite (V + L + H) coexistence (Driesner and Heinrich, 2007). (D) Violin plots showing the Kernel distribution of the $\log(CH_4/CO_2)$ values measured in global volcanic gases (Table S2) and volcanic gases from Vulcano crater fumaroles (Tables 1 and S1), as gray and red shaded areas, respectively.

5. Discussion

5.1. *Insights into the factors controlling CH_4 abundances in volcanic gases of Vulcano crater: concentration data vs. geochemical modeling*

The chemical and isotopic characteristics of the crater fumaroles from Vulcano Island have been extensively discussed in previous studies (e.g., Chiodini et al., 1993, Taran, 2011, Paonita et al., 2013 and references therein). Mixing and reaction controlled parameters have been identified based on temporal and spatial variabilities in geochemical data (Chiodini et al., 1993) (Figs. 3 and 4). The main gas constituents (H_2O and CO_2), the inert gases (He and N_2), the isotopic composition of CO_2 ($\delta^{13}C$) and, to a lesser extent, the isotopic composition of H_2O (δ^2H) and the relative H_2O CO_2 and S^{tot} (where $S^{tot} = SO_2 + H_2S$) concentrations, are interpreted to be fixed by the mixing between a magmatic and a hydrothermal component (Figs. 3A and 4). In contrast to the mixing-controlled parameters, minor reactive species (H_2 and CO) are controlled by temperature, pressure (i.e., water pressure, PH_2O) and redox conditions (fO_2). In particular, H_2 and CO abundances appear to be primarily governed by the SO_2-H_2S "magmatic" gas buffer (Giggenbach, 1987), at temperatures and pressures close to those of the surface vents (Fig. 3B.2 and B.4). However, deviations of measured $\log(CO/CO_2)$ and $\log(H_2/H_2O)$ concentration ratios from the equilibrium values, as observed in Fig. 3B.2 and B.4, reveal the occurrence of other processes. These departures may be due to quenching effects or to secondary control exerted by "hydrothermal" rock buffers (Giggenbach, 1987), probably FeO-$FeO_{1.5}$ and HM (hematite-magnetite) as suggested by their ability to enclose most of the compositional variability (Fig. 3B.2 and B.4).

Methane shows a more complex behavior. According to the hypothesis of a mixing between a CH_4-bearing hydrothermal and a magmatic component, the latter being basically devoid of CH_4, CH_4 and CO_2 are expected to show a negative correlation in a CO_2 vs. CH_4 biplot. To test this hypothesis, data are compared against a magmatic-hydrothermal binary mixing curve obtained assuming CH_4 and CO_2 concentrations of 1 and 50000 µmol/mol, and 0 and 300000 µmol/mol for hydrothermal and magmatic gases, respectively. As illustrated by the CO_2-CH_4 binary plot in Fig. 5A, CO_2 and CH_4 concentrations are not

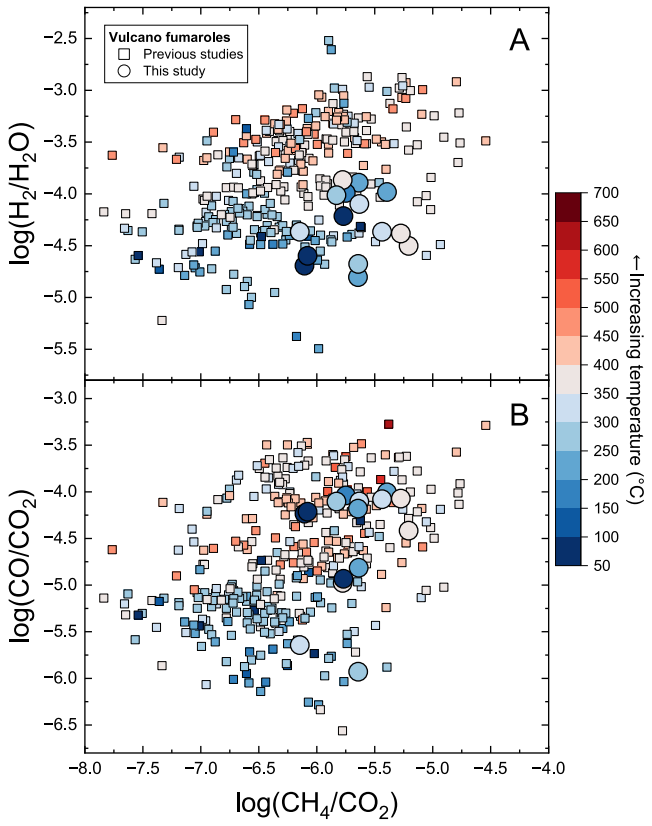

Fig. 6. Binary plots (A) log(CH_4/CO_2) vs log (H_2/H_2O), and (B) log(CH_4/CO_2) vs. log(CO/CO_2) for the fumaroles of the *La Fossa* crater of Vulcano Island. Data are from this study (Table 1) and previous measurements (Table S1). Different colors distinguish the measured outlet temperatures of the gas vents.

correlated and the data plot far from the mixing curve (gray curve in Fig. 5A). It is worth noting that using hydrothermal gases with considerably higher CH_4 concentrations (e.g., 50 μmol/mol; $CO_2/CH_4 = 10^3$) would not change the main outcome of the data vs. model comparison. Hence, mixing of a magmatic component that is devoid of methane and a hydrothermal component contributing all the methane cannot be regarded as the only responsible for the observed CH_4 variation.

Compared to H_2 and CO, CH_4 abundance shows a less clear correlation with venting temperature (Fig. 5B). Nevertheless, crater fumaroles with venting temperatures of 200–350 °C and > 350 °C exhibit CH_4 average concentration of 0.06 and 0.15 μmol/mol, respectively. Furthermore, despite the large dispersion of data, higher log(CH_4/CO_2) ratios seem to be associated with higher log(H_2/H_2O) and log(CO/CO_2) ratios (Fig. 6), which, in turn, are generally correlated with higher outlet temperatures (Fig. 3B).

However, after closely examining the scatterplots, it is not immediately apparent how these variables are correlated with each other. To make the interpretation easier, we decided to identify the variables or combination of variables that are responsible for the large observed variability in the data. Consequently, we conducted a correlation-based Principal Component Analysis (PCA) on a set of parameters (H_2O, CO_2, N_2, He, $\delta^{13}C$-CO_2, H_2, CO, CH_4 and fumarole vent temperature) in order to identify a group of linearly uncorrelated variables, referred to as principal components (PCs), and rank them based on their ability to control the variance. In our case, the firsts four PCs cumulatively retain 82.78 % of the total variance in the data, while the remaining PCs (PC5–PC9) explain only a minor fraction (<20 %) of the variance (Table 5; Fig. 7A). The results of the PCA show that the variance in the data is mainly governed by two different components: (1) PC1 explains 45.25 % of the variance and describes a dimension correlated with H_2O, CO_2, N_2, He and $\delta^{13}C$-CO_2; and (2) PC2 retains 20.62 % of the variance and delineates a dimension correlated with vent temperature, CH_4, H_2 and CO (Fig. 7B). These results clearly indicate that variables previously ascribed to magmatic-hydrothermal mixing processes contribute almost equally and exclusively to the PC1. The remaining variance in the data is instead mostly governed by the component PC2 (and also PC3 and PC4) which, in turn, appears to be mainly related to reactions controlled by T-PH_2O-fO_2 conditions. This finding supports the idea that CH_4 concentration from volcanic gases discharged at Vulcano crater is not controlled by the contribution of hydrothermal fluids to the magmatic ones (i.e., a simple binary mixing process), since other processes (e.g., chemical re-equilibration, oxidative conversion, contribution from multiple unknown sources) can strongly affect the CH_4 abundance.

By comparing the measured CH_4 contents, in the form of log(CH_4/CO_2) ratios, with those expected for chemical equilibrium with co-discharged CO_2 attained via the widely used Sabatier reaction ($CO_2 + 4H_2 = CH_4 + 2H_2O$; Giggenbach, 1997, Taran and Giggenbach, 2003) at different T-PH_2O-fO_2 conditions, we can get valuable insights on its origin and thermodynamic state in the volcanic gases. It is important to mention that recent findings have questioned the occurrence of overall fluid-mineral or fluid–fluid equilibria, suggesting, instead, that concentrations may rather reflect metastable equilibria or non-equilibrium conditions influenced by elemental fluxes, initial composition of fluids and rocks, and reaction pathways and progress (Stefánsson, 2017; Ricci et al., 2022). However, a comprehensive reactive transport model of the

Table 5
Principal Component Analysis (PCA) of H_2O, CO_2, N_2, He, $\delta^{13}C$-CO_2, T (fumarole vent temperature), H_2, CO and CH_4. "Percentage of variance" indicates the amount of the variation represented by the different eigenvalues. "Cumulative percentage" indicates the proportion of variance cumulatively retained by the eigenvalues.

	Eigenvectors								
Variables	PC1	PC2	PC3	PC4	PC5	PC6	PC7	PC8	PC9
H_2O	−0.48072	0.04698	−0.06617	−0.00707	0.14243	0.06476	0.30547	0.39569	0.6985
CO_2	0.47838	−0.0581	0.0839	0.01783	−0.14112	−0.09309	−0.32992	−0.33688	0.71379
N_2	0.32431	0.0639	−0.15845	0.41114	0.64933	0.52242	0.04374	−0.00466	0.01072
He	0.48019	−0.02623	0.01731	−0.04686	−0.11253	−0.0902	−0.17145	0.84528	−0.03914
$\delta^{13}C$-CO_2	0.42815	−0.00809	0.1	−0.10925	−0.19466	0.01985	0.8638	−0.09925	0.01989
T	0.02853	0.52299	−0.46151	−0.32204	−0.37638	0.50699	−0.09615	−0.02285	0.02222
H_2	−0.07087	0.49982	0.24673	0.73867	−0.36052	−0.07756	0.0301	0.04116	−0.00732
CO	0.12272	0.50553	−0.38827	−0.08819	0.36998	−0.65257	0.0695	−0.05726	−0.000117
CH_4	0.0091	0.459	0.72701	−0.39917	0.28124	0.12956	−0.07346	0.00834	−0.00174
Importance of components									
Eigenvalue	4.07287	1.85603	0.82573	0.69514	0.63466	0.57774	0.28404	0.05138	0.00242
Percentage of variance	45.25%	20.62%	9.17%	7.72%	7.05%	6.42%	3.16%	0.57%	0.03%
Cumulative percentage	45.25%	65.88%	75.05%	82.78%	89.83%	96.25%	99.40%	99.97%	100.00%

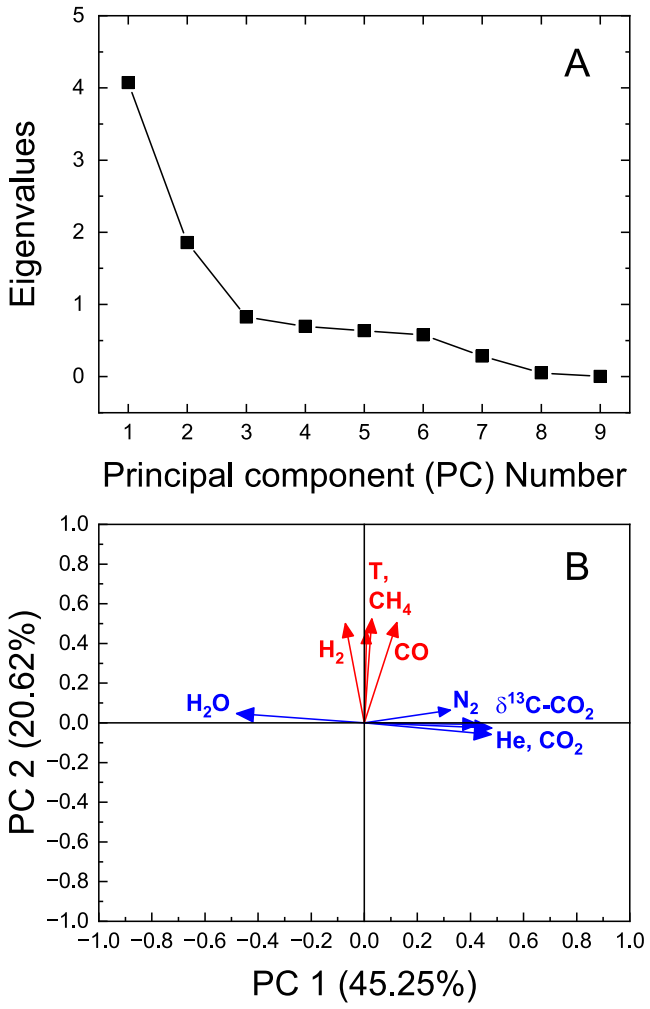

Fig. 7. Binary plots showing the results of the Principal Components Analysis (PCA) performed on data from this study (Tables 1 and 3) and previous studies (Table S1), and considering the following variables: fumarole vent temperature (T), concentrations of H_2O, CO_2, N_2, He, H_2, CO and CH_4, and isotopic composition of CO_2 ($\delta^{13}C$). In our case, nine PCs cumulatively retain the total variance (100 %) in the data (Table 5). The eigenvalues of the PCs are shown in panel (A). (B) Biplot of the PC1 versus PC2, with percentage of variance indicated in parentheses. The length of the vector from the origin indicates the variance of the variable. Concentrations of H_2O, CO_2, N_2 and He and $\delta^{13}C$-CO_2 contribute almost equally and exclusively to PC1 (blue vectors), while T and concentrations of H_2, CO and CH_4 mainly correlate with PC2.

magmatic-hydrothermal system of the *La Fossa* crater is not currently available, and building one was beyond the scope of this study. Therefore, for the following discussion, we decided to stick to the more "classical", yet robust, approach.

Vulcano gases show low CH_4 amounts (<1.5 μmol/mol; Tables 1 and S1), with $\log(CH_4/CO_2)$ ratios ranging from −7.8 to −4.5 (mean = −6.2, one standard deviation = 0.6), in agreement with the lowest values of the compositional range from other volcanic gases worldwide (Fig. 5D and Table S2). By studying the volcanic gases discharged from White Island (New Zealand), Giggenbach (1987) suggested that CH_4 may form in hydrothermal systems where rock-buffering conditions prevail and then remains quenched upon its entrainment into the rapidly ascending magmatic gas carrier. As suggested by previous studies (e.g., Chiodini et al., 1993, 1995; Nuccio et al., 1999; Di Liberto et al., 2002; Federico et al., 2010), at Vulcano, deep magmatic gases and hydrothermal fluids, before interacting with each other, are characterized by different T-PH_2O-fO_2 conditions. Accordingly, we have defined the conditions prevailing in the two source fluids as follows: (1) high temperatures and pressures (700–950 °C, 200 bar), redox conditions set by the SO_2-H_2S magmatic gas buffer, $SO_2/H_2S = 15$ (thick red curve in Fig. 5C), and (2) T-PH_2O fixed by vapor–liquid-halite coexistence and redox conditions fixed by hematite-magnetite (HM) redox buffer (dashed black curves in Fig. 5C). Inspection of Fig. 5C reveals that measured CH_4/CO_2 ratios of Vulcano gases are orders of magnitude higher than those predicted for deep magmatic gases. Similarly, measured $\log(CH_4/CO_2)$ ratios are also several orders of magnitude higher than theoretical values predicted by the attainment of equilibrium under hydrothermal conditions fixed by hematite-magnetite redox buffer. Furthermore, Fig. 5C shows that chemical re-equilibration upon cooling with rock buffers (e.g., FeO-$FeO_{1.5}$ or HM; black curves in Fig. 5C) should always lead to an increase in CH_4/CO_2 ratio with decreasing temperature, in clear opposition to what is indicated by the data. In fact, measured $\log(CH_4/CO_2)$ ratios and vent temperatures are positively correlated, crosscutting the rock-buffer equilibrium curves. Additionally, Fig. 5C shows that measured CH_4/CO_2 ratios are around 5–13 orders of magnitude higher than the theoretical values calculated at T-PH_2O-fO_2 conditions prevailing at the surface in the fumarolic gas discharges of Vulcano crater ($100 < T < 700$ °C, $PH_2O \approx 1$ bar, SO_2-H_2S redox buffer and $SO_2/H_2S = 0.5$; dashed red curve in Fig. 5C). Therefore, we conclude that CH_4/CO_2 ratios in the ascending and cooling volcanic gas carrier is not governed by chemical equilibria. It may follow that excess CH_4 is predominantly produced by processes that do not accompany CH_4-CO_2 equilibration, such as thermal cracking of organic matter or kinetically-controlled abiotic synthesis.

5.2. *Origin of large $\delta^{13}C$ and $\delta^{2}H$ variability of CH_4 in volcanic gases of Vulcano crater*

To further investigate the origin of CH_4 and the potential effects of post-genetic processes, the isotopic composition of CH_4 from Vulcano crater fumaroles is firstly compared to $\delta^{13}C$-$\delta^{2}H$ compositional fields conventionally ascribed to microbial, thermogenic, and abiotic CH_4 sources. (Milkov and Etiope, 2018). It is important to mention that the validity of such diagram to distinguish between different CH_4 sources has recently been questioned (e.g., Fiebig et al., 2019; Xia and Gao, 2022). In particular, Xia and Gao (2022) clearly demonstrated that abiotic signals can also be produced by thermal decomposition or microbial hydrogenolysis of organic matter. Therefore, close attention should be paid on the interpretation of such a plot. As shown in Fig. 8, some measured isotopic compositions apparently plot in the "abiotic field", while others could be associated with either thermogenesis or abiotic production or even require presently unknown formation mechanisms (Fig. 8). It is therefore evident that such approach provides inconclusive information on the origin of CH_4 in Vulcano crater gases. As illustrated in Fig. 8, the $\delta^{13}C$ and $\delta^{2}H$ values of Vulcano CH_4 are positively correlated, with the best linear fit having an angular coefficient of 25. Differences in data gathered from the same fumarole at different times (FNA fumarole, Fig. 8) point to a considerable temporal variability of the described isotopic characteristics and allowed to more robustly define the $\delta^{13}C$-$\delta^{2}H$ linear correlation which has a slope of 29. Furthermore, in our dataset we observe that as $\delta^{13}C$ and $\delta^{2}H$ of CH_4 increase, CH_4 concentrations decrease (Fig. 9). As reported by Etiope and Sherwood Lollar (2013), kinetic isotope fractionations, i.e., ^{13}C and ^{2}H enrichment in a residual fraction of CH_4, are associated with degradation and removal of CH_4 (e.g., microbial and abiotic oxidation). Apart from removal of methane, mixing of multiple CH_4 sources could in principle also generate data distributions as in Fig. 9. Therefore, two possible scenarios emerge: (1) mixing of multiple CH_4 sources, or (2) post-genetic alteration of single-sourced CH_4 characterized by extraordinary light isotopic signature.

5.2.1. *Assessment of the existence of multiple CH_4 sources*

The $\delta^{13}C$-$\delta^{2}H$ positive trend in Fig. 8 could reflect a mixing between two components. In fact, a binary mixing process in a $\delta^{13}C$-$\delta^{2}H$ diagram would produce a $\delta^{13}C$-$\delta^{2}H$ linear relationship. The observed variability

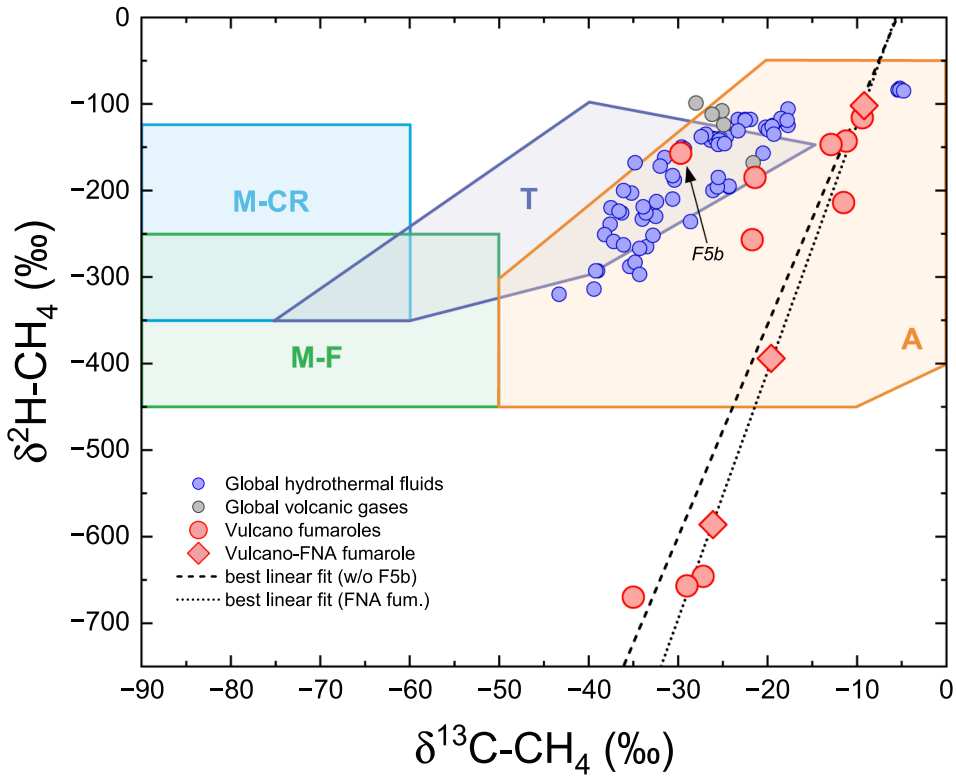

Fig. 8. Correlation plot between $\delta^{13}C$ and $\delta^{2}H$ for CH_4 from various natural sources. Methane from Vulcano fumaroles is shown. The equation of the best linear fit is as follow: $\delta^{2}H = 24.523 \times \delta^{13}C + 135.52$ (adj. $R^2 = 0.817$; Pearson's r = 0.91). This function was obtained by considering the whole dataset with the exception of fumarole F5b which displays an isotopic signature considerably departing from the main trend. It is worth noting that including this sample would not drastically change the statistical measures of the linear regression (adj. $R^2 = 0.55$; Pearson's r = 0.77). The equation of the best linear fit obtained taking into account isotopic data from FNA fumarole is as follow: $\delta^{2}H = 28.587 \times \delta^{13}C + 162.47$ (±7.68) (adj. $R^2 = 0.999$; Pearson's r = 0.9999). Fields characteristic for microbial (generated by carbonate reduction, M-CR, and fermentation, M-F), thermogenic and potentially abiogenic sources are drawn after Milkov and Etiope (2018). The isotopic composition of CH_4 from global volcanic gases (Table S2) and hydrothermal fluids (Fiebig et al., 2019) are also shown for comparison as gray and blue circles, respectively. The isotopic compositions are reported in delta notation (‰) relative to V-PDB and V-SMOW for carbon and hydrogen, respectively.

would then result from the variations in the relative contribution from each of these methane sources, in our case: (S1) a ^{13}C- and ^{2}H-enriched CH_4, and (S2) a ^{13}C- and ^{2}H-depleted CH_4.

Late addition of artificial CH_4 generated by CO/CO_2 hydrogenation at the metal-gas interface during the interaction of the fumarolic gases with the sampling titanium tube might constitute one end-member. However, tests made without using the titanium tube clearly demonstrate that such process, if it occurs at all, has no influence on the concentration ratios and stable isotope compositions of C_1-C_2 hydrocarbons (Table 4).

If methane bulk isotope compositions are plotted against methane concentration (Fig. 9), most data plots far from simple binary mixing curves, implying that the two end-members may exhibit variable methane concentrations and/or that $\delta^{2}H$-CH_4 is largely affected by secondary hydrogen isotope exchange with H_2O and/or H_2. In order to further evaluate the mixing hypothesis and following the approach firstly introduced by Bernard et al. (1978) for identifying microbial-thermogenic mixing in natural gases, the $^{13}C/^{12}C$ and $^{2}H/^{1}H$ ratios of CH_4 from Vulcano gases are plotted against CH_4/C_2H_6 ratios (Fig. 10A and B). Data distribution appears to follow hyperbolic mixing trends, especially if it is taken into consideration that ethene (C_2H_4) in the samples may fully derive from oxidation of ethane (C_2H_6) and assuming $\delta^{13}C$-CH_4 and $CH_4/(C_2H_4 + C_2H_6)$ ratios of samples most and least enriched in methane to be characteristic of the two end-members (Fig. 10C and D).

The S1 end-member has $\delta^{13}C$ and $\delta^{2}H$ values of CH_4 of −9.2 ‰ and −102 ‰, respectively. Furthermore, it shows carbon isotopic composition of the total C_2-fraction ($\delta^{13}C$-C_2^{tot}) of −16 ‰, and inverse carbon isotopic trend between C_1 and C_2^{tot} hydrocarbons (i.e., $\delta^{13}C$-$C_1 > \delta^{13}C$-C_2^{tot}). According to the genetic classification of Milkov and Etiope (2018), such characteristics would be ascribable to an abiotic origin. However, following the method described in Fiebig et al. (2019), late-stage (low fraction of residual organic precursor) open-system cracking of organic carbon of marine origin can also produce C_1-C_2 hydrocarbons with isotopic characteristics of S1 end-member (Fig. 11). Interestingly, gases discharged from the low-temperature (≤100 °C) subaerial and submarine gas vents along the *Levante* beach, at the foothills of the *La Fossa* cone (Fig. 1B; Capaccioni et al., 2001), displays isotopic compositions close to those of S1, with $\delta^{13}C$ and $\delta^{2}H$ average values of −5.1 ‰ and −84 ‰, respectively (Fiebig et al., 2019). Moreover, gases from the *Levante* beach have $\delta^{13}C$-C_2H_6 values similar to those of $\delta^{13}C$-C_2^{tot} of the S1 end-member, and exhibit marked C_1-C_2 inverse carbon isotope distribution patterns (Fiebig et al., 2019). These gas emissions are considered to be exclusively fed by a multi-layered hydrothermal system mainly recharged by external seawater with estimated reservoir temperatures as high as 400 °C in its deepest part (Federico et al., 2010). Accordingly, these might be further indications that S1 methane end-member is formed via high-temperature thermal cracking of marine organic carbon occurring within the deep seawater-fed hydrothermal reservoir enveloping the central volcanic edifice. The striking similarity in the isotopic signature of C_1-C_2 hydrocarbons between S1 end-member and the *Levante* gases might be indeed indicative of the entrainment of CH_4 from the hydrothermal envelope located at the foothill of the *La Fossa* cone. However, it is important to mention that gases discharged at the *Levante* beach have CH_4/C_2^{tot} 1–2 orders of magnitude higher than those inferred for the S1 end-member (Chiodini et al., 1995; Capaccioni et al., 2001). Should the S1 end-member originate from the hydrothermal envelope at *Levante*, these differences would

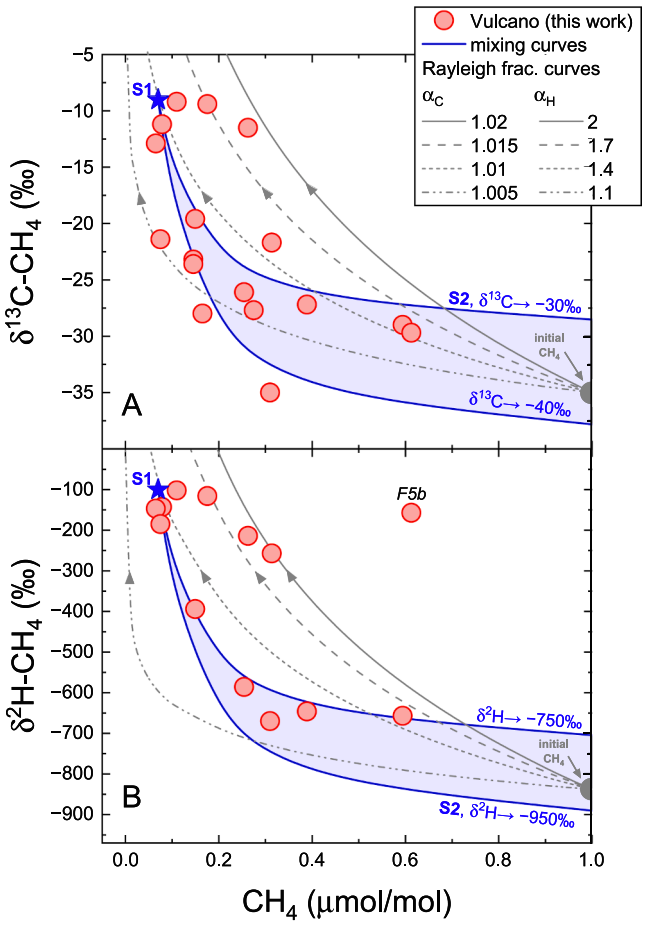

Fig. 9. Biplots of CH_4 concentrations vs. $\delta^{13}C$-CH_4 (A), and vs. δ^2H-CH_4 (B) for volcanic gases discharged at Vulcano crater. Measured data are compared with results from mixing (blue curves) and Rayleigh fractionation (gray curves) modeling. The curves of mixing between two different CH_4 sources, S1 and S2, are computed solving the following equation: $\delta_{MIX} = [CH_4]_{S1}/[CH_4]_{MIX} \times (\delta_{S1} - \delta_{S2}) + \delta_{S2}$. In our model the CH_4-low (0.07 μmol/mol) S1 source is characterized by $\delta^{13}C$ and δ^2H of CH_4 of –9 ‰ and –100 ‰, respectively. The S2 source is defined as a CH_4-rich component (>1 μmol/mol) and with $\delta^{13}C$-CH_4 and δ^2H-CH_4 ranging from –40 and –30 ‰ and from –950 and –750 ‰, respectively. The Rayleigh fractionation model describes the change of CH_4 concentration and isotopic signatures from an arbitrarily selected initial conditions (gray half-circle) as the CH_4 consumption reaction proceeds (i.e., fraction of remaining CH_4) and in function of the kinetic carbon and hydrogen isotope fractionation factors (α_C and α_H). The Rayleigh function can be approximated by the general form (Coleman et al., 1981): $\delta_t = \delta_i + 1000 \times (1/\alpha - 1) \times \ln(f)$; where δ is the isotopic composition in delta notation of initial (i) CH_4 ($\delta^{13}C = -35$ ‰ and $\delta^2H = -838$ ‰) and that at time t (t); f is the fraction of initial substrate remaining at time t, and α is the kinetic isotope fractionation factor.

indicate that methane has been preferentially removed or ethane been preferentially added on its way and entrainment into the *La Fossa* system.

The origin of the remarkably ^{13}C- and ^2H-depleted methane source S2 is discussed in more detail in Section 5.3.

5.2.2. *Evaluation of the effect of post-genetic alteration processes on single-sourced CH_4*

5.2.2.1. Isotopic re-equilibration in the CH_4-CO_2-H_2O system. As shown in Fig. 12, the most ^{13}C- and ^2H-enriched CH_4 samples plot close to the theoretical curve of CH_4-CO_2-H_2O isotopic equilibrium at around 700 °C. This equilibration temperature is roughly in agreement with those inferred by Nuccio et al. (1999), using mass and energy balance equations, for the magmatic-hydrothermal mixing zone (T = 600–650 °C, PH_2O = 200 bar). Hence, the observed data distribution in Fig. 12 could be interpreted as a progressive attainment of isotopic equilibrium of the CH_4-CO_2-H_2O system at high-temperatures (≥700 °C) starting from out-of-equilibrium signals (i.e., ^{13}C- and ^2H-depleted CH_4 samples). However, in the $\delta^{13}C$ vs. δ^2H diagram, such process would be described by a linear function only if the kinetics of ^2H-^1H and ^{13}C-^{12}C exchange for CH_4-H_2O and CH_4-CO_2, respectively, were the same. Based on experiments performed at different temperatures, expressions for the temperature dependence of carbon and hydrogen isotope equilibrium fractionation factors and for isotopic exchange rates between CH_4 and CO_2 (Giggenbach, 1997, Horita, 2001, Kueter et al., 2019) and CH_4 and H_2O (e.g., Reeves et al., 2012, Wang et al., 2018, Turner et al., 2022), respectively, have been devided. As suggested by Beaudry et al. (2021), rates of carbon exchange between CO_2 and CH_4 are expected to be much slower than those of hydrogen exchange between H_2O and CH_4, with, for example, rate constants, as $\log(k^i)$, at 700 °C of −2.4 and +1.57 yr^{-1} for the former and the latter, respectively. Accordingly, as shown in Fig. 12, data distribution cannot be explained by a progressive attainment of isotope equilibrium at high temperatures from an initial disequilibrium condition. This is in accordance with findings of Sato et al. (2002) who did not observe isotopic equilibrium between CH_4 and CO_2 in the fumarolic gases from Satsuma-Iwojima volcano (Japan), even where venting temperatures exceeded 800 °C. Moreover, Giggenbach (1997) estimated that the rate of attainment of isotopic equilibrium between CO_2 and CH_4 is 400 times slower than that of CO_2-CH_4 chemical equilibration. Hence, the absence of co-occurring CH_4-CO_2 chemical and isotopic equilibrium in the Vulcano gases strongly implies that near-equilibrium isotope fractionation observed for some samples might be coincidental.

5.2.2.2. Thermochemical sulfate reduction (TSR) and abiogenic methane oxidation (AMO). As stated by Taran and Giggenbach (2003), CH_4 transported in the gas phase may undergo oxidative conversion via numerous reaction pathways when in contact with oxides and at elevated temperatures (>400 °C). Methane can also be oxidized by sulfate (e.g., aqueous SO_4^{2-}, anhydrite) in high-temperature (>200 °C) hydrothermal aquifers during a process called thermochemical sulfate reduction (TSR; He et al., 2020 and references therein). Abiogenic methane oxidation (AMO) in the presence of metal oxides and TSR lead to enrichment of remaining CH_4 in ^{13}C and ^2H with kinetic isotope effects controlling the isotopic composition of residual CH_4 (e.g., Kiyosu and Imaizumi, 1996, He et al., 2020). The relative changes of isotope concentrations during AMO, expressed as ΔH/ΔC values, are 11.5 and 20.9 for AMO in the presence of MnO_2 at 400 and 200 °C, respectively, and –2.5 at 400–530 °C for AMO mediated by Fe_2O_3 (Kiyosu and Imaizumi, 1996). These two trends are reported in Fig. 12 as AMO(1) and AMO(2), respectively. In a series of lab experiments of TSR of CH_4 at temperature of 400–575 °C, He et al. (2020) observed that kinetic isotope effect governs the ^{13}C content of CH_4, while no evident ^2H enrichments were observed. This resulted in an increase of ^{13}C coupled with broadly constant ^2H contents of residual CH_4 during TSR of CH_4 (TSR(2) in Fig. 12). Other authors (e.g., Milkov and Etiope, 2018) reported instead a slight hydrogen fractionation during CH_4 TSR (TSR(1) in Fig. 12). Ratios of hydrogen and carbon kinetic fractionation factors, expressed as ΔH/ΔC, are 1 and ≈3.7 for TSR reported by He et al. (2020) and Milkov and Etiope (2018), respectively. The isotopic data distribution of CH_4 from Vulcano crater fumaroles follows a linear trend having a slope (i.e., ΔH/ΔC) of ≈24–29 (Fig. 8), considerably higher than those reported for TSR and AOM in the previous studies. This evidence likely rules out AMO or TSR to be responsible for the observed isotopic variability of Vulcano crater fumaroles.

5.2.2.3. Heteroatomic reactions: sulfonation and chlorination. Degradation of CH_4 in the gas-phase at elevated temperatures via sulfonation involving typical volcanic species (e.g., SO_2 and H_2S) was suggested as a

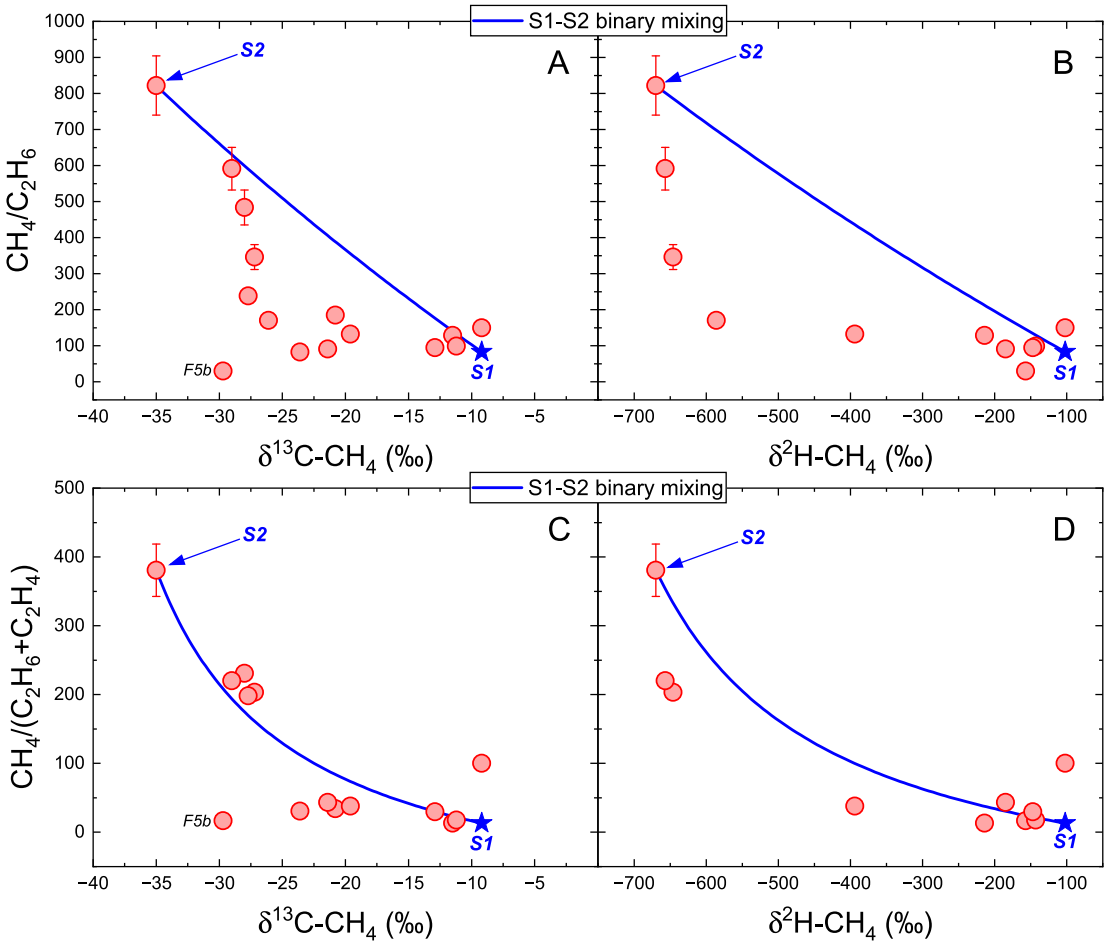

Fig. 10. CH_4/C_2H_6 and $CH_4/(C_2H_4 + C_2H_6)$ ratios in function of CH_4 isotopes ($\delta^{13}C$ and δ^2H). Mixing curves are drawn by assuming the end-members to have the following chemical and isotopic composition: (S1) $CH_4 = 0.07$ μmol/mol, $CH_4/C_2H_6 = 83$, $CH_4/(C_2H_4 + C_2H_6) = 13$, $\delta^{13}C\text{-}CH_4 = -9.2$ ‰, $\delta^2H\text{-}CH_4 = -102$ ‰, and (S2) $CH_4 = 0.6$ μmol/mol, $CH_4/C_2H_6 = 822$, $CH_4/(C_2H_4 + C_2H_6) = 381$, $\delta^{13}C\text{-}CH_4 = -35$ ‰, $\delta^2H\text{-}CH_4 = -670$ ‰ When the entire C_2 fraction is considered in the mixing modeling, mixing curves better compare with the observed natural variability (see panels C and D). The S1-S2 binary mixing curves are generated following the equations described in Bini et al. (2022).

possible reaction pathway for the formation of carbon disulfide (CS_2) in Vulcano gases (Schwandner et al., 2013). The irreversible CH_4 sulfonation could be responsible for the observed enrichment in ^{13}C and ^2H and co-occurring decrease of CH_4 abundance (Fig. 9). These authors reported much lower concentrations of S-substituted relative to Cl-substituted volatile organic compounds in Vulcano fumaroles. Indeed, these authors found significant amounts (few to tens of nmol/mol) of dichloromethane (CH_2Cl_2) and trichloromethane ($CHCl_3$). The formation of these Cl-substituted compounds was ascribed to free radical substitution of gaseous molecular chlorine (Cl_2) for hydrogen atoms in CH_4. Similarly, Tassi et al. (2012) reported the occurrence of chlorinated hydrocarbons in Vulcano gases from extra-atmospheric volcanogenic sources. Zelenski and Taran (2012) detected 2–60 ppm-vol. of Cl_2 in volcanic emissions of Central Kamchatka and suggested catalytic oxidation of volcanic HCl and oxidative decomposition of chloroferrates as Cl_2 formation mechanisms. Interestingly, Vulcano gases contain up to >1000 μmol/mol of HCl (Table 1) and the occurrence of metal-chloride complexes have been inferred by several authors (e.g., Wahrenberger. 1997, Chiaradia et al., 2018). Substitution of H-atoms with Cl-atoms in the CH_4 structure is expected to cause a kinetic isotope effect because such process involves the breakage of relatively stable C—H bonds. Generally, $^{13}C—^2H$ and $^{12}C—^2H$ bonds are more stable than $^{13}C—^1H$ and $^{12}C—^1H$ bonds, respectively. Thus, during chlorination $^{13}C—^1H$ and $^{12}C—^1H$ bonds are preferentially broken when compared to those of $^{13}C—^2H$ and $^{12}C—^2H$, respectively. In a series of lab experiments, Strunin et al. (1975) observed that the ratio of the rate constants k_{1H}/k_{2H} (i.e., the kinetic isotope fractionation factor α_H), measured for the reaction of atomic chlorine with C^1H_4 and C^2H_4 at temperatures >200 °C, was much >1 (e.g., around 3 at 300 °C) and inversely correlated with temperature. Therefore, strong kinetic hydrogen isotope fractionation is expected during CH_4 chlorination. Similarly, several studies (e.g., Strode et al., 2020, Thanwerdas et al., 2022) on the reaction of CH_4 oxidation by chlorine atoms in the atmosphere at low temperatures (≤24 °C) observed a strong carbon kinetic isotope effect, with, for example, kinetic isotope fractionation factors as high as 1.066 at 24 °C (Saueressig et al., 1995). As a result, such hydrogen and carbon kinetic isotope fractionations will leave the unreacted residual CH_4 enriched in ^2H and ^{13}C. We are aware that these observations are related to a different environment and are, hence, possibly not applicable to hot volcanic gases. However, even though the magnitude of the kinetic isotope effects may change at high temperatures and in the presence of HCl and other gas species, the general direction of the fractionation (i.e., heavy isotopes enrichment) is not expected to drastically change. Interestingly, using a Rayleigh fractionation model (Figs. 9 and 12) and considering relatively high CH_4 abundances (1 μmol/mol) and ^{12}C-, ^1H-enriched compositions (–35 ‰ and –838 ‰, respectively) as initial conditions, we can indeed reproduce the $\delta^{13}C\text{-}CH_4$ and $\delta^2H\text{-}CH_4$ values and CH_4 concentrations of the Vulcano crater gases when carbon and hydrogen kinetic fractionation factors (α_C and α_H, respectively) are significantly >1. For example, by considering a conservative value of α_H equal to 2, Rayleigh fractionation modeling can reproduce most of the observed isotopic variability when α_C ranges between 1.015 and 1.020 (Fig. 12). It

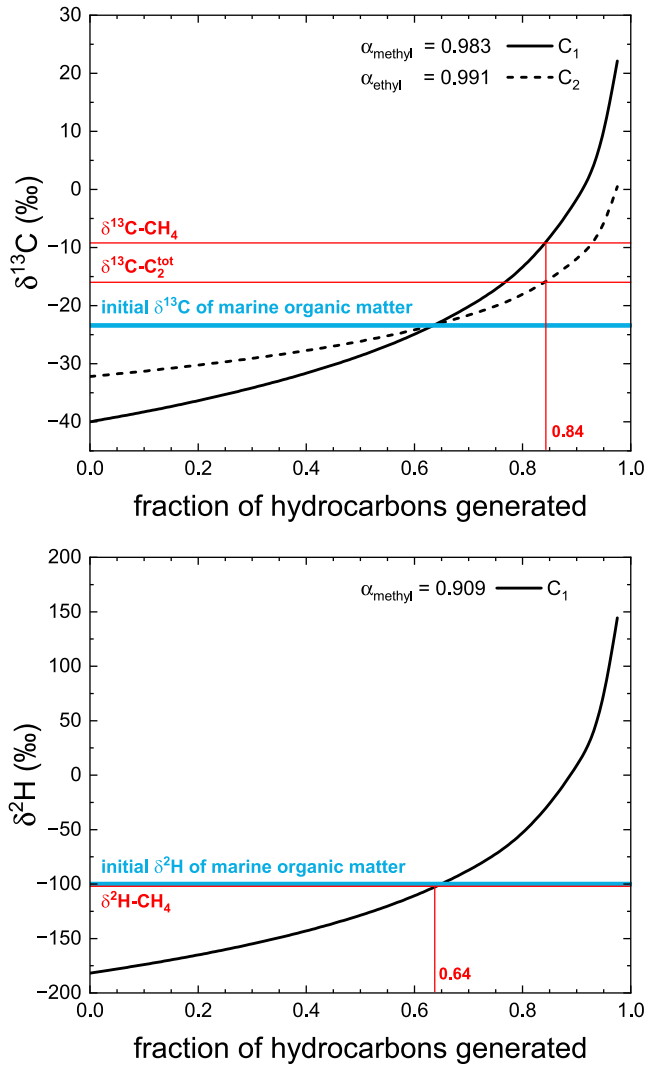

Fig. 11. Carbon and hydrogen isotopic composition of instantaneously produced C_1 and C_2 hydrocarbons as a function of the fraction of hydrocarbons generated via open-system cracking of marine organic matter. Large fractions of generated hydrocarbons (≥0.64) are required to match the isotopic composition of the most isotopically enriched CH_4 and C_2^{tot} in Vulcano fumaroles. For open system cracking of marine organic matter, carbon and hydrogen fractionation factors between CH_4 and its precursor site are set to 0.983 and 0.909, respectively; as constrained from pyrolysis experiments of marine kukersite (Berner et al. 1995). Carbon isotope fractionation factor between C_2 and its precursor site is set to 0.991 according to experimental results of Berner et al. (1995). Carbon and hydrogen isotopes of initial marine organic matter were selected as follows: $\delta^{13}C$ of − 23.4 ‰, equal to the average composition of DOC (dissolved organic carbon) in the Tyrrhenian Sea (Santinelli et al., 2015), and δ^2H of –100 ‰ corresponding to the average hydrogen isotopic composition of marine DOC (Schoell, 1984).

is plausible, therefore, to conclude that chlorination reaction of CH_4 may explain the trend of decreasing concentrations and ^{12}C and ^1H contents of CH_4 observed in the Vulcano gases. However, it is important to emphasize that experimental studies on the occurrence and effects of CH_4 chlorination in volcanic gases are presently lacking. Thus, more information on the kinetic isotope effect of Cl-substitution on CH_4 and the determination of abundances and isotopes of both CH_4 and heteroatomic compounds in volcanic gases are required to prove/disprove this hypothesis.

5.3. Extraordinary ^{13}C- and ^2H-depleted CH_4 in Vulcano crater gases: evidence of abiogenic methane formation?

All the scenarios described in the previous sections have a lowest common denominator: an extraordinary ^{13}C- and ^2H-depleted CH_4 is required as CH_4 source. As far as known, δ^2H-CH_4 values below − 500 ‰ have not still been related to natural sources (Fig. 8). However, they are mentioned in connection with artificial CH_4 generated via a process called “drill-bit metamorphism” (DBM) during borehole drilling (Faber et al., 1988, Whiticar, 1990, Wenger et al., 2009, Strąpoć et al., 2020) and with experimental Fischer-Tropsch-type (FTT) abiotic CH_4 synthesis under hydrothermal conditions (McCollom et al., 2010). The former occurrence has been related to cracking of oil-based drilling mud under high temperatures (up to 1200 °C), pressures and strain rates at the interface between the metal-surface of the drill-bit, rock and drilling fluids during borehole perforation (Wenger et al., 2009). Accordingly, it may be possible that similar ^2H-depleted CH_4 is formed owing to thermal cracking of organic matter hosted in sedimentary rocks or transported by circulating groundwater at extreme conditions within the magmatic-hydrothermal system of Vulcano. However, such ^2H-depleted values have never been generated by pyrolysis experiments (e.g., Berner et al., 1995) or reported in modeling of open-system cracking of organic matter under hydrothermal conditions (e.g., Fiebig et al., 2019), with lowest $^2H/^1H$ ratios of CH_4 commonly being around −200 to −300 ‰. In order to generate CH_4 with δ^2H values < −600 ‰ via open-system cracking, assuming an initial δ^2H of the organic matter of −100 ‰ (Fiebig et al., 2019), the hydrogen isotope fractionation factor between instantaneously produced CH_4 and its precursor site (α_H) has to be <0.444. Such threshold is considerably lower than values of α_H, reported in open-system pyrolysis experiments, of 0.8333–0.9090 (Berner et al., 1995). Accordingly, thermogenesis seems unlikely and mechanisms other than cracking of organic matter may be needed to explain the origin of ^2H-depleted CH_4.

In a series of catalyzed FTT hydrothermal experiments with CO as carbon source, McCollom et al. (2010) abiotically generated CH_4 with $^2H/^1H$ ratio < −450 ‰ and found very similar values of δ^2H between H_2 and CH_4, indicating that little to no fractionation occurred during the abiogenic CH_4 formation. Similarly, Taran et al. (2010) observed negligible isotope fractionation between initial H_2 and generated CH_4 during open-system experiments of CO hydrogenation at 255 °C in the presence of iron (Fe) as catalyst. Furthermore, isotopic data on the δ^2H values of C_1–C_3 alkanes produced during closed-system aqueous FTT experiments at 400 °C and 500 bars (Fu et al., 2007) suggest that alkanes (including methane) form with relatively minor kinetic H isotope fractionation relative to H_2. Analogously to results of FTT experiments, two Vulcano gases show little hydrogen isotopic fractionation ($\alpha_{H2\text{-}CH4}$) between H_2 and CH_4 ($\alpha_{H2\text{-}CH4}$ = 1.05–1.38). However, hydrogen isotopic composition of H_2 at Vulcano varies greatly: from −638 to −299 ‰ (Table 3). Given the fast hydrogen isotope exchange between H_2 and H_2O at high temperatures (Pester et al., 2018, Ricci et al., 2022), values around −325 ± 25 ‰ can be explained with the attainment of isotopic equilibrium between H_2 and H_2O at 360–450 °C, close to measured venting temperatures. On the contrary, δ^2H-H_2 < −500 ‰ (i.e., $\alpha_{H2O\text{-}H2}$ > 2) gives apparent equilibrium temperatures of 80–190 °C, lower than the sampling temperatures. Some sort of kinetic effect has to be invoked to explain such low values. Recently, results of multi-component thermochemical modelling by Henley and Fischer (2021) showed that R_H [i.e., $\log(fH_2/fH_2O)$] of volcanic gases can be affected by reaction progress and kinetics of gas-solids interactions (e.g., $CaAl_2Si_3O_8 + 2SO_2 + 2H_2 = CaSO_4 + Al_2SiO_5 + SiO_2 + H_2O + H_2S$) and rock-surface/volcanic gas ratio (i.e., fracture network of fumarolic conduits). Accordingly, it is plausible that, during such gas–solid reactions, kinetic isotope fractionation occurs, leading to ^1H enrichment of H_2 in the volcanic gases. Furthermore, it is also possible that the presence of H_2O in the dry gas samples might have triggered unwanted after-sampling hydrogen isotope exchange reactions between H_2, H_2O and H_2S in the gas storage

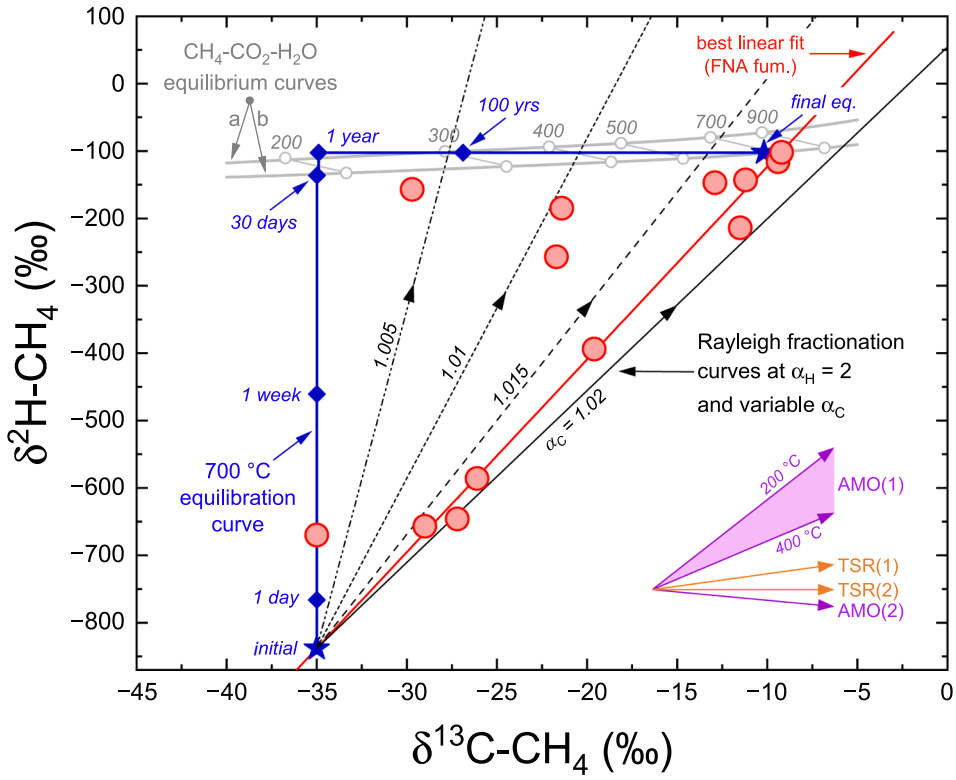

Fig. 12. Correlation plot between $\delta^{13}C$ and $\delta^{2}H$ for CH_4 from Vulcano fumaroles. Vulcano data are compared with results from equilibrium and kinetic modeling. The best linear fit of Vulcano data (FNA-only function), whose equation is reported in Fig. 8, is also shown. Carbon and hydrogen isotopic compositions of CH_4 in equilibrium with CO_2 and H_2O at different temperatures are shown as solid gray curves (a and b). Such curves were calculated assuming isotopic equilibrium with (a) hydrothermal fluids having $\delta^{13}C\text{-}CO_2 = -3$ ‰ and $\delta^{2}H\text{-}H_2O = +10$ ‰, and (b) magmatic volatiles having $\delta^{13}C\text{-}CO_2 = 0$ ‰ and $\delta^{2}H\text{-}H_2O = -15$ ‰. The equilibrium isotopic composition of CH_4 was obtained using the T-α equations provided by Horita (2001) and Turner et al. (2022) for CO_2-CH_4 and H_2O-CH_4 system, respectively. The blue curve describes the progressive attainment of CH_4-CO_2-H_2O isotopic equilibrium at 700 °C starting from out-of-equilibrium conditions (blue star). Methane isotopic composition at different times (1 day, 1 week, 30 days, 1 year and 100 years) are shown for reference. The initial CH_4 isotopic signature ($\delta^{13}C = -35$ ‰; $\delta^{2}H = -838$ ‰) was arbitrarily selected along the best linear fit. Rates of isotopic exchange between CH_4 and H_2O and CH_4 and CO_2 at 700 °C were calculated using equations reported by Turner et al. (2022) and Beaudry et al. (2021), respectively, and by assuming PH_2O of 200 bars and steam density equal to 2.6267 mol/L (calculated at 200 bars and 700 °C). The results of the Rayleigh fractionation modeling are reported as black curves. The initial carbon and hydrogen isotopic compositions of CH_4 used in our Rayleigh modeling were − 35 ‰ ($\delta^{13}C$) and −838 ‰ ($\delta^{2}H$), respectively (blue star) The Rayleigh fractionation curves are drawn by fixing the kinetic hydrogen isotope fractionation factor (α_H) at 2 and making the kinetic carbon isotope fractionation factor (α_C) varies from 1.005 to 1.02. The isotopic effect of abiogenic methane oxidation (AMO) in the presence of MnO_2 at 200 and 400 °C [AMO(1)] and Fe_2O_3 [AMO(2)] is reported as purple arrows (Kiyosu and Imaizumi 1996). The isotopic effect of thermochemical sulfate reduction (TSR) is reported as TSR(1) and TSR(2) orange arrows with slopes according to considerations from Milkov and Etiope (2018) and He et al. (2020), respectively.

vessels at room temperature, which would result in a decrease of the original $\delta^{2}H\text{-}H_2$ values if H_2O was still the dominant-bearing constituent in the dry gases. Hence, at this time, profound conclusions on CH_4 formation mechanisms cannot solely be drawn on the basis of CH_4-H_2 hydrogen isotope fractionation.

Carbon isotope measurements of FTT experiments at ≥245 °C indicate that abiotically generated CH_4 is considerably depleted in ^{13}C compared to the initial carbon source (CO or CO_2) with $\Delta^{13}C$ (i.e., $\delta^{13}C\text{-}CO_2/CO - \delta^{13}C\text{-}CH_4$) values roughly ranging from +20 to +60 ‰ (Fu et al., 2007, Taran et al., 2007, 2010, McCollom et al., 2010). Moreover, during open-system catalytic CO_2 hydrogenation experiments at 245–350 °C, Taran et al. (2010) observed little (2–6 ‰) carbon isotope fractionation between CH_4 and C_2H_6 and almost no difference in the carbon isotopic composition among the C_2—C_5 hydrocarbons. Similarly, Taran et al. (2007), in a series of open-system catalyzed CO hydrogenation experiments at 260–310 °C, observed that carbon isotope fractionation between CH_4 and C_2H_6 changes from +6 to –2 ‰ as the CO conversion into hydrocarbons increases. Interestingly, Vulcano gases with $\delta^{2}H\text{-}CH_4 < -600$ ‰ show $\Delta^{13}C$ (CO_2—CH_4) between +26.7 and +34.3 ‰ and $\Delta^{13}C$ (CH_4—C_2^{tot}) of −2.1 ‰ (Table 3), which are well comparable with the results obtained by hydrothermal experiments involving FTT synthesis. It is worth noting that a strong isotope fractionation ($\Delta^{13}C > 30$ ‰) between CO_2 and CH_4 was also observed for extremely high temperature (up to 882 °C) volcanic gases of the Satsuma-Iwojima volcano in Japan (Sato et al., 2002). Here, extremely ^{12}C-enriched CH_4 (-55.9 ‰ $\leq \delta^{13}C \leq -36.9$ ‰) was found, possibly indicating that abiotic CH_4 at Vulcano might have carbon and hydrogen pristine isotopic signatures considerably lighter than those measured in our study. Also, the finding of measurable concentrations of considerably ^{12}C-enriched CH_4 in 855 °C volcanic gases at Satsuma-Iwojima volcano (Japan; Sato et al., 2002) indicate that abiotic synthesis may occur at close-to-magmatic temperatures. At these sites, additional collection/analysis of gases and investigation of $\delta^{2}H\text{-}CH_4$ and $\delta^{2}H\text{-}H_2$ are necessary to understand if strong depletion in ^{13}C and ^{2}H might be characteristic of methane abiotically formed at temperatures intermediate between those characteristic of magmatic (>900 °C) and hydrothermal (<450 °C) conditions.

6. Conclusions

High-temperature volcanic gases discharged at the *La Fossa* crater of Vulcano Island offer the unique opportunity of studying the origin and reactions of CH_4 under magmatic and hydrothermal conditions. The sampled fumarolic gases display a wide range in CH_4 concentration (0.07–0.61 μmol/mol) and $\delta^{13}C$ and $\delta^{2}H$ values of CH_4, showing a positive linear correlation and varying from −35 to −9.2 ‰ vs. V-PDB

and −670 to −102 ‰ vs. V-SMOW, respectively. Our study reveals that CH_4, contrary to other parameters such as the H_2O-CO_2-N_2-He subsystem, is not controlled by mixing processes between magmatic volatiles, devoid of methane, and gases supplied by circulating hydrothermal fluids. Furthermore, comparison of data with geochemical models highlights that CH_4 concentrations considerably exceed those defined by theoretical equilibria expected for T-PH_2O-fO_2 conditions prevailing at the surface discharge, in deeper parts of the magmatic gases and in the hydrothermal envelope. However, the dataset and the performed PCA analysis demonstrate that CH_4 abundances are positively correlated with venting temperatures and H_2 and CO contents of the fumarolic gases. Moreover, gases showing extremely negative $\delta^{13}C$-CH_4 and $\delta^{2}H$-CH_4 values systematically display higher CH_4 abundances.

In an attempt to reconcile our chemical and isotopic observations, we propose two possible scenarios: (1) mixing of two CH_4 sources having extremely different isotopic signatures, and (2) post-genetic alteration of single-sourced CH_4 characterized by an extraordinarily light initial isotopic composition. With respect to scenario (1), CH_4 showing the most ^{13}C- and ^{2}H-enriched compositions (i.e., −9.2 ‰ and −102 ‰, respectively) might be supplied to the crater fumaroles by the entrainment of small amounts of thermogenic CH_4 formed in seawater-sourced hydrothermal fluids. Such CH_4 variably mixes with isotopically light CH_4 within the fumarolic conduits before being discharged to the atmosphere. Comparison with available isotopic data from naturally occurring and artificially produced CH_4, seems to rule out a thermogenic origin for the isotopically light end-member. We speculate that this end-member CH_4 is formed at high, possibly close-to-magmatic, temperatures and under reducing conditions by kinetically-controlled catalytic reduction of CO (or CO_2) by H_2 during ascent towards the surface of hot magmatic gases interacting with mineral surfaces. Such conditions might help overcoming the strong activation barriers of the abiotic synthesis of CH_4 and allow the reaction steps involved in the CO/CO_2 hydrogenation to proceed. According to scenario (2), instead, the isotopically light abiotic methane, once formed at extremely high temperatures, undergoes substantial post-genetic degradation (coupled with strong isotopic fractionation) during its ascent towards the surface.

Our investigation suggests that conditions favorable for abiotic formation of CH_4 via kinetically-controlled CO/CO_2 hydrogenation might be encountered in the deep roots of magmatic-hydrothermal systems and that the so formed abiotic CH_4 may have an isotopic signature well distinguishable from that of CH_4 encountered in purely-hydrothermal fluids, with extreme deuterium depletion being the most notable feature. Further investigations of methane in high-temperature volcanic gases are necessary to test this hypothesis.

Declaration of Competing Interest

The authors declare that they have no known competing financial interests or personal relationships that could have appeared to influence the work reported in this paper.

Data availability

Data are available through Mendeley Data at: https://doi.org/10.17632/k2xtnr4k6h.1.

Acknowledgments

The first step of this research project was made possible thanks to a mini-grant awarded by the Deep Energy Community (DEC) of the DCO (Deep Carbon Observatory) to Franco Tassi (Lead-PI) in August 2016. Furthermore, this work was financially supported by the Stable Isotopes Laboratory (Resp. Jens Fiebig) of the Goethe University and the Laboratory of Fluid Geochemistry (Resp. Franco Tassi) of the University of Florence. We are very grateful to Christoph Schreiber, Jacopo Cabassi, Stefania Venturi and Chiara Caponi for their help in gas sampling and analysis, for the thoughtful discussions about Vulcano Island, volcanic gases and methane geochemistry and for the fun times we shared in the field and in the lab. We sincerely thank Yuri Taran, Jabrane Labidi and an anonymous reviewer for their constructive comments and suggestions which improved the quality of the manuscript. We wish to thank Shuhei Ono for careful editorial handling. This study has been developed in the framework of the PhD thesis "*Geochemistry of C-bearing gas compounds in natural fluids under crustal conditions: insights into deep and shallow processes*" (A. Ricci, University of Bologna).

Appendix A. Supplementary material

The Supplementary Material contains a compilation of data from previous published studies on the chemical composition and stable isotopes of volcanic gases discharged from high-temperature fumaroles at the *La Fossa* crater of Vulcano Island (Table S1). In addition, a detailed survey of published data of outlet gas temperature, methane and carbon dioxide concentrations and stable isotopic composition of CH_4, H_2, H_2O, CO_2 and CO of volcanic gases from active volcanic systems worldwide is also reported in Table S2. Corresponding references are also reported. Supplementary material to this article can be found online at https://doi.org/10.1016/j.gca.2023.10.019.

References

Aiuppa, A., Federico, C., Giudice, G., Gurrieri, S., 2005. Chemical mapping of a fumarolic field: La Fossa Crater, Vulcano Island (Aeolian Islands, Italy). Geophys. Res. Lett. 32, L13309.

Aiuppa, A., Bitetto, M., Calabrese, S., Delle Donne, D., Lages, J., La Monica, F.P., Chiodini, G., Tamburello, G., Cotterill, A., Fulignati, P., Gioncada, A., Liu, E.J., Moretti, R., Pistolesi, M., 2022. Mafic magma feeds degassing unrest at Vulcano Island, Italy. Commun. Earth Environ. 3 (1), 255.

Beaudry, P., Stefánsson, A., Fiebig, J., Rhim, J.H., Ono, S., 2021. High temperature generation and equilibration of methane in terrestrial geothermal systems: Evidence from clumped isotopologues. Geochim. Cosmochim. Acta 309, 209–234.

Bernard, B.B., Brooks, J.M., Sackett, W.M., 1978. Light hydrocarbons in recent Texas continental shelf and slope sediments. J. Geophys. Res. 83, 4053–4061.

Berner, U., Faber, E., Scheeder, G., Panten, D., 1995. Primary cracking of algal and landplant kerogens: kinetic models of isotope variations in methane, ethane and propane. Chem. Geol. 126, 233–245.

Bini, G., Chiodini, G., Caliro, S., Tassi, F., Vaselli, O., Rizzo, A.L., Mollo, S., Vougioukalakis, G.E., Bachmann, O., 2022. Nitrogen, helium, and argon reveal the magmatic signature of fumarole gases and episodes of outgassing from upper-crustal magma reservoirs: The case of the Nisyros caldera (Aegean Arc, Greece). Geochim. Cosmochim. Acta 335, 68–84.

Cannata, A., Diliberto, S., Alparone, S., Gambino, S., Gresta, S., Liotta, M., Madonia, P., Milluzzo, V., Aliotta, M., Montalto, P., 2012. Multiparametric approach in investigating volcanohydrothermal systems: the case study of Vulcano (Aeolian Islands, Italy). Pure Appl. Geophys. 169, 167–182.

Capaccioni, B., Tassi, F., Vaselli, O., 2001. Organic and inorganic geochemistry of low temperature gas discharges at the Baia di Levante beach, Vulcano Island, Italy. J. Volcanol. Geotherm. Res. 108 (1–4), 173–185.

Capaccioni, B., Taran, Y., Tassi, F., Vaselli, O., Mangani, G., Macias, J.L., 2004. Source conditions and degradation processes of light hydrocarbons in volcanic gases: an example from El Chichón volcano (Chiapas State, Mexico). Chem. Geol. 206 (1–2), 81–96.

Capasso, G., Favara, R., Inguaggiato, S., 1997. Chemical features and isotopic composition of gaseous manifestations on Vulcano Island, Aeolian Islands, Italy: an interpretative model of fluid circulation. Geochim. Cosmochim. Acta 61 (16), 3425–3440.

Capasso, G., Favara, R., Francofonte, S., Inguaggiato, S., 1999. Chemical and isotopic variations in fumarolic discharge and thermal waters at Vulcano Island (Aeolian Islands, Italy) during 1996: evidence of resumed volcanic activity. J. Volcanol. Geoth. Res. 88 (3), 167–175.

Capasso, G., D'Alessandro, W., Favara, R., Inguaggiato, S., Parello, F., 2001. Interaction between the deep fluids and the shallow groundwaters on Vulcano Island (Italy). J. Volcanol. Geoth. Res. 108 (1–4), 187–198.

Capasso, G., Federico, C., Madonia, P., Paonita, A., 2014. Response of the shallow aquifer of the volcano-hydrothermal system during the recent crises at Vulcano Island (Aeolian Archipelago, Italy). J. Volcanol. Geoth. Res. 273, 70–80.

Carapezza, M., Nuccio, P.M., Valenza, M., 1981. Genesis and evolution of the fumaroles of Vulcano (Aeolian Islands, Italy): a geochemical model. Bull. Volcanol. 44, 547–563.

Casalbore, D., Romagnoli, C., Bosman, A., De Astis, G., Lucchi, F., Tranne, C.A., Chiocci, F.L., 2019. Multi-stage formation of La Fossa Caldera (Vulcano Island, Italy) from an integrated subaerial and submarine analysis. Mar. Geophys. Res. 40 (4), 479–492.

Chiaradia, M., Pujol-Solà, N., Farré-de-Pablo, J., Aiuppa, A., Paonita, A., Rizzo, A.L., Brusca, L., 2018. Geochemistry and isotope composition (Sr, Pb, δ^{66}Zn) of Vulcano fumaroles (Aeolian Islands, Italy). Chem. Geol. 493, 153–171.
Chiodini, G., 2009. CO_2/CH_4 ratio in fumaroles a powerful tool to detect magma degassing episodes at quiescent volcanoes. Geophys. Res. Lett. 36 (2).
Chiodini, G., Cioni, R., Marini, L., 1993. Reactions governing the chemistry of crater fumaroles from Vulcano Island, Italy, and implications for volcanic surveillance. Appl. Geochem. 8, 357–371.
Chiodini, G., Cioni, R., Marini, L., Panichi, C., 1995. Origin of the fumarolic fluids of Vulcano Island, Italy and implication for volcanic surveillance. Bull. Volcanol. 57, 99–110.
Chiodini, G., Frondini, F., Raco, B., 1996. Diffuse emission of CO_2 from the Fossa crater, Vulcano Island (Italy). Bull. Volcanol. 58, 41–50.
Chiodini, G., Allard, P., Caliro, S., Parello, F., 2000. ^{18}O exchange between steam and carbon dioxide in volcanic and hydrothermal gases: implications for the source of water. Geochim. Cosmochim. Acta 64, 2479–2488.
Cioni, R., D'Amore, F., 1984. A genetic model for the crater fumaroles of Vulcano Island (Sicily, Italy). Geothermics 13, 375–384.
Coleman, D.D., Risatti, J.B., Schoell, M., 1981. Fractionation of carbon and hydrogen isotopes by methane-oxidizing bacteria. Geochim. Cosmochim. Acta 45 (7), 1033–1037.
De Astis, G., La Volpe, L., Peccerillo, A., Civetta, L., 1997. Volcanological and petrological evolution of Vulcano island (Aeolian Arc, southern Tyrrhenian Sea). J. Geophys. Res. 102 (B4), 8021–8050.
Di Liberto, V., Nuccio, P.M., Paonita, A., 2002. Genesis of chlorine and sulphur in fumarolic emissions at Vulcano Island (Italy): assessment of pH and redox conditions in the hydrothermal system. J. Volcanol. Geoth. Res. 116 (1–2), 137–150.
Di Martino, R.M.R., Gurrieri, S., Camarda, M., Capasso, G., Prano, V., 2022. Hazardous changes in soil CO_2 emissions at Vulcano, Italy, in 2021. J. Geophys. Res.: Solid Earth 127 (11).
Diliberto, I.S., 2017. Long-term monitoring on a closed-conduit volcano: A 25 year long time-series of temperatures recorded at La Fossa cone (Vulcano Island, Italy), ranging from 250 °C to 520 °C. J. Volcanol. Geoth. Res. 346, 151–160.
Diliberto, I.S., Cangemi, M., Gagliano, A.L., Inguaggiato, S., Jacome Paz, M.P., Madonia, P., Mazot, A., Pedon, M., Pisciotta, A., 2021. Volcanic Gas Hazard Assessment in the Baia di Levante Area (Vulcano Island, Italy) Inferred by Geochemical Investigation of Passive Fluid Degassing. Geosciences 11 (11), 478.
Driesner, T., Heinrich, C.A., 2007. The system H_2O–NaCl. Part I: Correlation formulae for phase relations in temperature–pressure–composition space from 0 to 1000 °C, 0 to 5000 bar, and 0 to 1 X_{NaCl}. Geochim. Cosmochim. Acta 71 (20), 4880–4901.
Etiope, G., Sherwood Lollar, B., 2013. Abiotic methane on Earth. Rev. Geophys. 51 (2), 276–299.
Faber, E., Gerling, P., Dumke, I., 1988. Gaseous hydrocarbons of unknown origin found while drilling. Org Geochem. 13 (4–6), 875–879.
Federico, C., Capasso, G., Paonita, A., Favara, R., 2010. Effects of steam-heating processes on a stratified volcanic aquifer: Stable isotopes and dissolved gases in thermal waters of Vulcano Island (Aeolian archipelago). J. Volcanol. Geoth. Res. 192 (3–4), 178–190.
Federico, C., Cocina, O., Gambino, S., Paonita, A., Branca, S., Coltelli, M., Italiano, F., Bruno, V., Caltabiano, T., Camarda, M., Capasso, G., De Gregorio, S., Diliberto, I.S., Di Martino, R.M.R., Falsaperla, S., Greco, F., Pecoraino, G., Salerno, G., Sciotto, M., Bellomo, S., Grazia, G.D., Ferrari, F., Gattuso, A., La Pica, L., Mattia, M., Pisciotta, A. F., Pruiti, L., Sortino, F., 2023. Inferences on the 2021 Ongoing Volcanic Unrest at Vulcano Island (Italy) through a Comprehensive Multidisciplinary Surveillance Network. Remote Sens. (Basel) 15 (5), 1405.
Fiebig, J., Chiodini, G., Caliro, S., Rizzo, A.L., Spandenberg, J., Hunziker, J.C., 2004. Chemical and isotopic equilibrium between CO_2 and CH_4 in fumarolic gas discharges: generation of CH_4 in arc magmatic–hydrothermal systems. Geochim. Cosmochim. Acta 68, 2321–2334.
Fiebig, J., Woodland, A.B., Spangenberg, J., Oschmann, W., 2007. Natural evidence for rapid abiogenic hydrothermal generation of CH_4. Geochim. Cosmochim. Acta 71, 3028–3039.
Fiebig, J., Hofmann, S., Tassi, F., D'Alessandro, W., Vaselli, O., Woodland, A.B., 2015. Isotopic patterns of hydrothermal hydrocarbons emitted from Mediterranean volcanoes. Chem. Geol. 396, 152–163.
Fiebig, J., Stefansson, A., Ricci, A., Tassi, F., Viveiros, F., Silva, S., Lopez, T.M., Schreiber, C., Hofmann, S., Mountain, B.W., 2019. Abiogenesis not required to explain the origin of volcanic-hydrothermal hydrocarbons. Geochem. Persp. Lett. 11, 23–27.
Fu, Q., Lollar, B.S., Horita, J., Lacrampe-Couloume, G., Seyfried Jr, W.E., 2007. Abiotic formation of hydrocarbons under hydrothermal conditions: Constraints from chemical and isotope data. Geochim. Cosmochim. Acta 71 (8), 1982–1998.
Giggenbach, W.F., 1987. Redox processes governing the chemistry of fumarolic gas discharges from White Island, New Zealand. Appl. Geochem. 2 (2), 143–161.
Giggenbach, W.F., 1992. Isotopic shift in waters from geothermal and volcanic systems along convergent plate boundaries and their origin. Earth Planet. Sci. Lett. 113, 495–510.
Giggenbach, W.F., 1995. Variations in the chemical and isotopic composition of fluids discharged from the Taupo Volcanic Zone, New Zealand. J. Volcanol. Geotherm. Res. 68 (1–3), 89–116.
Giggenbach, W.F., 1997. Relative importance of thermodynamic and kinetic processes in governing the chemical and isotopic composition of carbon gases in high-heat flow sedimentary basins. Geochim. Cosmochim. Acta 61, 3763–3785.
Giggenbach, W.F., Tedesco, D., Sulistiyo, Y., Caprai, A., Cioni, R., Favara, R., Fischer, T. P., Hirabayashi, J.-I., Korzhinsky, M., Martini, M., Menyailov, I., Shinohara, H., 2001. Evaluation of results from the fourth and fifth IAVCEI field workshops on volcanic gases, Vulcano Island, Italy and Java, Indonesia. J. Volcanol. Geotherm. Res. 108 (1–4), 157–172.
Granieri, D., Carapezza, M.L., Chiodini, G., Avino, R., Caliro, S., Ranaldi, M., Ricci, T., Tarchini, L., 2006. Correlated increase in CO_2 fumarolic content and diffuse emission from La Fossa crater (Vulcano, Italy): evidence of volcanic unrest or increasing gas release from a stationary deep magma body? Geophys. Res. Lett. 33, L13316.
Harris, A., Alparone, S., Bonforte, A., Dehn, J., Gambino, S., Lodato, L., Spampinato, L., 2012. Vent temperature trends at the Vulcano Fossa fumarole field: the role of permeability. Bull. Volcanol. 74, 1293–1311.
He, K., Zhang, S., Wang, X., Mi, J., Hu, G., 2020. Hydrothermal experiments involving methane and sulfate: insights into carbon isotope fractionation of methane during thermochemical sulfate reduction. Org. Geochem. 149, 104101.
Henley, R.W., Fischer, T.P., 2021. Sulfur sequestration and redox equilibria in volcanic gases. J. Volcanol. Geoth. Res. 414, 107181.
Horita, J., 2001. Carbon isotope exchange in the system CO_2-CH_4 at elevated temperatures. Geochim. Cosmochim. Acta 65 (12), 1907–1919.
Inguaggiato, S., Diliberto, I.S., Federico, C., Paonita, A., Vita, F., 2018. Review of the evolution of geochemical monitoring, networks and methodologies applied to the volcanoes of the Aeolian Arc (Italy). Earth Sci. Rev. 176, 241–276.
Inguaggiato, S., Vita, F., Diliberto, I.S., Mazot, A., Calderone, L., Mastrolia, A., Corrao, M., 2022. The extensive parameters as a tool to monitoring the volcanic activity: The case study of Vulcano Island (Italy). Remote Sens. (Basel) 14 (5), 1283.
Inostroza, M., Tassi, F., Aguilera, F., Sepúlveda, J.P., Capecchiacci, F., Venturi, S., Capasso, G., 2020. Geochemistry of gas and water discharge from the magmatic-hydrothermal system of Guallatiri volcano, northern Chile. Bull. Volcanol. 82 (7), 1–16.
Italiano, F., Pecoraino, G., Nuccio, P.M., 1998. Steam output from fumaroles of an active volcano: tectonic and magmatic-hydrothermal controls on the degassing system at Vulcano (Aeolian arc). J. Geophys. Res.: Solid Earth 103 (B12), 29829–29842.
Kiyosu, Y., 1983. Hydrogen isotopic compositions of hydrogen and methane from some volcanic areas in northeastern Japan. Earth Planet. Sci. Lett. 62 (1), 41–52.
Kiyosu, Y., Imaizumi, S., 1996. Carbon and hydrogen isotope fractionation during oxidation of methane by metal oxides at temperatures from 400° to 530°C. Chem. Geol. 133, 279–287.
Kueter, N., Schmidt, M.W., Lilley, M.D., Bernasconi, S.M., 2019. Experimental determination of equilibrium CH_4–CO_2–CO carbon isotope fractionation factors (300–1200 °C). Earth Planet. Sci. Lett. 506, 64–75.
Leeman, W.P., Tonarini, S., Pennisi, M., Ferrara, G., 2005. Boron isotope variations in fumarolic condensates and thermal waters from Vulcano Island, Italy: implications for evolution of volcanic fluids. Geochim. Cosmochim. Acta 69, 143–163.
Magro, G., Pennisi, M., 1991. Noble gases and nitrogen: mixing and temporal evolution in the fumarolic fluids of Vulcano,Italy. J. Volcanol. Geotherm. Res. 47 (3–4), 237–247.
Mandarano, M., Paonita, A., Martelli, M., Viccaro, M., Nicotra, E., Millar, I.L., 2016. Revealing magma degassing below closed-conduit active volcanoes: geochemical features of volcanic rocks versus fumarolic fluids at Vulcano (Aeolian Islands, Italy). Lithos 248, 272–287.
Martini, M., Tonani, F., 1970. Risultati del rilevamento geochimico: Vulcano 1969. Palermo.
Martini, M., Piccardi, G., Cellini, Legittimo, P., 1980. Geochemical surveillance of active volcanoes: data on the fumaroles of Vulcano (Aeolian Islands, Italy). Bull. Volcanol. 43, 255–263.
McCollom, T.M., 2013. Laboratory simulations of abiotic hydrocarbon formation in earth's deep subsurface. Rev. Mineral. Geochem. 75, 467–494.
McCollom, T.M., 2016. Abiotic methane formation during experimental serpentinization of olivine. Proc. Natl. Acad. Sci. 113, 13965–13970.
McCollom, T.M., Lollar, B.S., Lacrampe-Couloume, G., Seewald, J.S., 2010. The influence of carbon source on abiotic organic synthesis and carbon isotope fractionation under hydrothermal conditions. Geochim. Cosmochim. Acta 74 (9), 2717–2740.
Milkov, A.V., Etiope, G., 2018. Revised genetic diagrams for natural gases based on a global dataset of >20,000 samples. Org Geochem. 125, 109–120.
Montegrossi, G., Tassi, F., Vaselli, O., Buccianti, A., Garofalo, K., 2001. Sulfur species in volcanic gases. Anal. Chem. 73 (15), 3709–3715.
Nicotra, E., Giuffrida, M., Viccaro, M., Donato, P., D'Oriano, C., Paonita, A., De Rosa, R., 2018. Timescales of pre-eruptive magmatic processes at Vulcano (Aeolian Islands, Italy) during the last 1000 years. Lithos 316, 347–365.
Nuccio, P.M., Paonita, A., Sortino, F., 1999. Geochemical modeling of mixing between magmatic and hydrothermal gases: the case of Vulcano, Italy. Earth Planet. Sci. Lett. 167, 321–333.
Paonita, A., Favara, R., Nuccio, P.M., Sortino, F., 2002. Genesis of fumarolic emissions as inferred by isotope mass balances: CO_2 and water at Vulcano Island, Italy. Geochim. Cosmochim. Acta 66, 759–772.
Paonita, A., Federico, C., Bonfanti, P., Capasso, G., Inguaggiato, S., Italiano, F., Madonia, P., Pecoraino, G., Sortino, F., 2013. The episodic and abrupt geochemical changes at La Fossa fumaroles (Vulcano Island, Italy) and related constraints on the dynamics, structure, and compositions of the magmatic system. Geochim. Cosmochim. Acta 120, 158–178.
Pester, N.J., Conrad, M.E., Knauss, K.G., DePaolo, D.J., 2018. Kinetics of D/H isotope fractionation between molecular hydrogen and water. Geochim. Cosmochim. Acta 242, 191–212.
Reeves, E.P., Seewald, J.S., Sylva, S.P., 2012. Hydrogen isotope exchange between n-alkanes and water under hydrothermal conditions. Geochim. Cosmochim. Acta 77, 582–599.
Ricci, A., Kleine, B.I., Fiebig, J., Gunnarsson-Robin, J., Kamunya, K.M., Mountain, B., Stefánsson, A., 2022. Equilibrium and kinetic controls on molecular hydrogen

abundance and hydrogen isotope fractionation in hydrothermal fluids. Earth Planet. Sci. Lett. 579, 117338.
Salas-Navarro, J., Stix, J., de Moor, J.M., 2022. A new Multi-GAS system for continuous monitoring of CO_2/CH_4 ratios at active volcanoes. J. Volcanol. Geoth. Res. 426, 107533.
Santinelli, C., Follett, C., Brogi, S.R., Xu, L., Repeta, D., 2015. Carbon isotope measurements reveal unexpected cycling of dissolved organic matter in the deep Mediterranean Sea. Mar. Chem. 177, 267–277.
Sato, M., Tsunogai, U., Ishibashi, J.I., Notsu, K., Wakita, H., 1999. Carbon isotope measurement of extremely low amounts of CH_4: Application to volcanic gases from Satsuma-Iwojima,Japan. Anal. Sci. 15 (6), 513–516.
Sato, M., Mori, T., Shimoike, Y., Nagao, K., Notsu, K., 2002. Carbon isotope systematics of CO_2, CO and CH_4 in fumarolic gases from Satsuma-Iwojima volcanic island, Japan. Earth Planets Space 54 (3), 257–263.
Saueressig, G., Bergamaschi, P., Crowley, J.N., Fischer, H., Harris, G.W., 1995. Carbon kinetic isotope effect in the reaction of CH_4 with Cl atoms. Geophys. Res. Lett. 22 (10), 1225–1228.
Schoell, M., 1984. Wasserstoff- und Kohlenstoffisotope in organischen Substanzen, Erdölen und Erdgasen. Geol. Jahrb. D67, 1–161.
Schwandner, F.M., Seward, T.M., Giże, A.P., Hall, K., Dietrich, V.J., 2013. Halocarbons and other trace heteroatomic organic compounds in volcanic gases from Vulcano (Aeolian Islands, Italy). Geochim. Cosmochim. Acta 101, 191–221.
Selva, J., Bonadonna, C., Branca, S., De Astis, G., Gambino, S., Paonita, A., Pistolesi, M., Ricci, T., Sulpizio, A., Tibaldi, A., Ricciardi, A., 2020. Multiple hazards and paths to eruptions: A review of the volcanic system of Vulcano (Aeolian Islands, Italy). Earth Sci. Rev. 207, 103186.
Sessions, A.L., Burgoyne, T.W., Hayes, J.M., 2001. Determination of the H_3 factor in hydrogen isotope ratio monitoring mass spectrometry. Anal. Chem. 73, 200–207.
Sicardi, L., 1941. Il recente ciclo dell'attività fumarolica dell'isola di Vulcano. Bollettino Vulcanologico 7, 85–140.
Stefánsson, A., 2017. Gas chemistry of Icelandic thermal fluids. J. Volcanol. Geoth. Res. 346, 81–94.
Strapoć, D., Jacquet, B., Torres, O., Khan, S., Inan Villegas, E., Albrecht, H., Okoh, B., McKinney, D., 2020. Deep biogenic methane and drilling-associated gas artifacts: Influence on gas-based characterization of petroleum fluids. AAPG Bull. 104 (4), 887–912.
Strode, S.A., Wang, J.S., Manyin, M., Duncan, B., Hossaini, R., Keller, C.A., Michel, S.E., White, J.W., 2020. Strong sensitivity of the isotopic composition of methane to the plausible range of tropospheric chlorine. Atmos. Chem. Physics 20 (14), 8405–8419.
Strunin, V.P., Serdyuk, N.K., Chesnokov, E.N., Panfilov, V.N., 1975. Kinetic isotope effect in the chlorination of methane. React. Kinet. Catal. Lett. 3 (1), 97–104.
Symonds, R.B., Gerlach, T.M., Reed, M.H., 2001. Magmatic gas scrubbing: implications for volcano monitoring. J. Volcanol. Geoth. Res. 108 (1–4), 303–341.
Taran, Y.A., 2011. N_2, Ar, and He as a tool for discriminating sources of volcanic fluids with application to Vulcano, Italy. Bull. Volcanol. 73 (4), 395–408.
Taran, Y.A., Giggenbach, W.F., 2003. Geochemistry of light hydrocarbons in subduction-related volcanic and hydrothermal fluids. Soc. Econ. Geol. Special Publ. 10 (6), 61–74.
Taran, Y.A., Pilipenko, V.P., Rozhkov, A.M., Vakin, E.A., 1992. A geochemical model for fumaroles of the Mutnovsky volcano, Kamchatka, USSR. J. Volcanol. Geotherm. Res. 49 (3–4), 269–283.
Taran, Y.A., Kliger, G.A., Sevastianov, V.S., 2007. Carbon isotope effects in the open-system Fischer-Tropsch synthesis. Geochim. Cosmochim. Acta 71 (18), 4474–4487.
Taran, Y.A., Kliger, G.A., Cienfuegos, E., Shuykin, A.N., 2010. Carbon and hydrogen isotopic compositions of products of open-system catalytic hydrogenation of CO_2: Implications for abiogenic hydrocarbons in Earth's crust. Geochim. Cosmochim. Acta 74 (21), 6112–6125.
Tassi, F., Capecchiacci, F., Cabassi, J., Calabrese, S., Vaselli, O., Rouwet, D., Pecoraino, G., Chiodini, G., 2012. Geogenic and atmospheric sources for volatile organic compounds in fumarolic emissions from Mt. Etna and Vulcano Island (Sicily, Italy). J. Geophys. Res.: Atmos. 117, D17305.
Tedesco, D., Scarsi, P., 1999. Intensive gas sampling of noble gases and carbon at Vulcano (Southern Italy). J. Geophys. Res.: Solid Earth 104, 10499–10510.
Thanwerdas, J., Saunois, M., Pison, I., Hauglustaine, D., Berchet, A., Baier, B., Sweeney, C., Bousquet, P., 2022. How do Cl concentrations matter for the simulation of CH_4 and $\delta^{13}C(CH_4)$ and estimation of the CH_4 budget through atmospheric inversions? Atmos. Chem. Physics. 22 (23), 15489–15508.
Turner, A.C., Pester, N.J., Bill, M., Conrad, M.E., Knauss, K.G., Stolper, D.A., 2022. Experimental determination of hydrogen isotope exchange rates between methane and water under hydrothermal conditions. Geochim. Cosmochim. Acta 329, 231–255.
Vaselli, O., Tassi, F., Montegrossi, G., Capaccioni, B., Giannini, L., 2006. Sampling and analysis of fumarolic gases. Acta Vulcanol. 18 (1–2), 65–76.
Wahrenberger, C.M., 1997. Some aspects of the chemistry of volcanic gases. Doctoral dissertation ETH. No. 12252. ETH, Zurich.
Wang, D.T., Reeves, E.P., McDermott, J.M., Seewald, J.S., Ono, S., 2018. Clumped isotopologue constraints on the origin of methane at seafloor hot springs. Geochim. Cosmochim. Acta 223, 141–158.
Wenger, L.M., Pottorf, R.J., Macleod, G., Otten, G., Dreyfus, S., Justwan, H.K., Wood, E. S., 2009. Drill bit metamorphism: Recognition and impact on show evaluation: Society of Petroleum Engineers Annual Technical Conference and Exhibition, New Orleans, Louisiana, October 4–7, 2009, SPE-125218-MS, 9 p.
Whiticar, M.J., 1990. A geochemical perspective of natural gas and atmospheric methane. Org. Chem. 16 (1–3), 531–547.
Xia, X., Gao, Y., 2022. Validity of geochemical signatures of abiotic hydrocarbon gases on Earth. J. Geol. Soc. 179 (3).
Zanon, V., Frezzotti, M.L., Peccerillo, A., 2003. Magmatic feeding system and crustal magma accumulation beneath Vulcano Island (Italy): evidence from CO_2 fluid inclusions in quartz xenoliths. J. Geophys. Res.: Solid Earth 108 (B6), 2298.
Zelenski, M., Taran, Y.A., 2012. Volcanic emissions of molecular chlorine. Geochim. Cosmochim. Acta 87, 210–226.
Zelenski, M., Chaplygin, I., Babadi, M.F., Taran, Y., Campion, R., Mehrabi, B., Shakeri, A., Delavari, M., Nekrylov, N., Pokrovsky, B., Sevastyanov, V., Kuznetsova, O., 2020. Volcanic gas emissions from Taftan and Damavand, the Iranian volcanoes. J. Volcanol. Geoth. Res. 397, 106880.